

Super-resolution Algorithms for Joint Range-Azimuth-Doppler Estimation in Automotive Radars

Yalın Gürcan

Technische Universiteit Delft

SUPER-RESOLUTION ALGORITHMS FOR JOINT RANGE-AZIMUTH-DOPPLER ESTIMATION IN AUTOMOTIVE RADARS

by

Yalın Gürcan

in partial fulfillment of the requirements for the degree of

Master of Science

in Electrical Engineering

at the Delft University of Technology,

to be defended publicly on Wednesday January 25, 2017 at 10:00 AM.

Supervisor:	Prof. dr. A. Yarovoy	
Thesis committee:	Dr. O. Krasnov,	TU Delft
	Prof. dr. ir. G. Leus,	TU Delft
	Dr. F. Uysal,	TU Delft

An electronic version of this thesis is available at <http://repository.tudelft.nl/>.

The cover image is El Lissitzky's Proun 30, taken from

<https://www.wikiart.org/en/el-lissitzky/proun-30-1920>

ABSTRACT

In FMCW radar systems, spectral estimation methods are used to determine the beat frequency of the reflected signal in order to obtain information about the range of scatterers relative to the position of the transmit/receive elements. Array processing techniques take advantage of the phase shifts per element and likewise use spectral estimation methods to determine angle information. Range-Doppler processing methods utilize the Doppler shifts per chirp caused by the motion of the reflector to estimate the radial velocities relative to the position of the receiver.

The problem of estimation of these three parameters of scatterers in an area can then be simplified as a problem of spectral estimation over three separate domains. The recent algorithms for solving such a problem in the context of array based radar applications range from adaptive, nonparametric methods, subspace based parametric methods and sparse recovery methods. However, these methods mostly ignore the inter- and intra- pulse Doppler effects of multiple moving targets. Furthermore, with demand for more resolution, investigation of wideband effects on range-azimuth-Doppler estimation is necessary.

In this thesis, we firstly develop a MATLAB based MIMO radar simulator, on which the theoretical models are to be tested. The first aim of the thesis is to investigate the joint range-azimuth estimation methods and the shortcomings of narrowband assumptions, especially on the DoA estimation problem. We propose a novel signal model specifically for LFMCW radar systems and two methods of joint estimation using this model.

The next aim is to investigate the effects of the movement of the targets on accuracy of the estimation problem. We study these effects firstly on the range-azimuth estimation problem and provide a more detailed signal model, which, theoretically also allows for the joint estimation of range, azimuth and velocity parameters using only a single chirp. Then we look into joint estimation in three domains and provide a subspace based algorithm, using the proposed signal model, capable of solving this problem.

The accuracy of the new signal model and performance of the estimation algorithm is then tested on data generated by the MATLAB based simulator. Comparisons are made with respect to state of the art, MUSIC based joint estimation algorithm and theoretical bounds. Furthermore, range-Doppler estimation is performed on real life data, taken from the Dolphin prototype NXP automotive radar system. Future works based on this model is proposed.

ACKNOWLEDGEMENTS

Looking back at the day I received the mail stating my conditional application to the MSc programme at TU Delft, and reflecting upon my ecstatic reactions, I probably wouldn't have expected to feel the same way as this day, now that I am finally about to graduate after two (and a half) years. Not that I am feeling any less jovial about the situation; I am still grateful that my efforts thus far have allowed me to be accepted by and graduate from such a highly respected institute such as TU Delft. It is simply the fact that I wouldn't have imagined the hardships of obtaining this degree and all the skills and experiences gained by doing so.

In the period of this two (and a half) years, I have met so many wonderful people who have been there for me, helped me, suffered through my (mostly drunk) inane ramblings and guided me in my studies. I would like to show my gratitude towards all of them. Firstly, to my supervisors Prof. Yarovoy and Dr. Krasnov, for all their guidance and support in my thesis, also for their encouragement and emotional support when I was feeling the worst due to difficulties in my studies. Moreover, I would like to thank all the lovely people of the MS3 group; specifically, to Dr. Faruk Uysal and PhD student Shengzhi Xu for their help in my work. Secondly I would like to show gratitude to all my friends here in Delft, who made life much more enjoyable in a place far from home.

I would like to also thank all my friends back at home. Even though they were most of the time many many miles away from me, thanks to the wonders of the internet and VoIP they were able to keep me company nonetheless.

Finally, I would like to thank my family for their belief in me, in my skills, that I would overcome all the challenges I faced during my studies.

But above all, my deepest gratitude goes to my lovely sister. I say this without any exaggeration and with all my sincerity that without her constant support, her wise advices and her encouragement, I simply couldn't have made it here.

Yalın Gürcan
Delft, January 2017

CONTENTS

List of Figures	ix
List of Tables	xi
1 Introduction	1
1.1 Motivation	1
1.2 Research Goals	2
1.3 Structure and Approach.	2
2 Problem Formulation and Literature Survey	5
2.1 Problem Description	5
2.2 Current Approaches to DoA Estimation.	13
2.2.1 MVDR (Capon).	13
2.2.2 APES.	13
2.2.3 Subspace based methods	14
2.3 Conclusions.	17
3 FMCW Automotive Radar Simulator	19
3.1 Basics	19
3.2 System Model.	19
3.3 Environment	20
3.4 Transmitter	20
3.5 Receiver.	25
3.6 Conclusions.	27
4 Target Localization Using Wideband LFM CW Signals	29
4.1 Joint Delay-Angle Estimation	30
4.2 New Signal Model.	33
4.3 Proposed Methods	36
4.3.1 Phase Compensation of Movement of Targets in Subsequent Sweeps	37
4.3.2 Time Dependent Steering Vectors	37
4.4 Conclusions.	39

5	Moving Target Localization and Joint Range-Azimuth-Velocity Estimation	41
5.1	Range-Azimuth-Doppler Processing	41
5.2	Doppler Shift on Array Elements	43
5.3	Single Sweep Velocity Estimation	46
5.4	Conclusions.	46
6	Performance Evaluation	49
6.1	Effect of SNR on Estimation Accuracy.	49
6.2	Effect of Sweep Bandwidth on Estimation Accuracy.	50
6.3	Effect of Position of Scatterers on Estimation Accuracy	51
6.4	Application on Experimental Data	52
6.5	Conclusions.	54
7	Conclusions	55
7.1	Future Works	56
	Bibliography	57

LIST OF FIGURES

2.1	Simplified spectrum of the transmit and receive signals of LFM CW radar	7
2.2	A Range-Doppler plot obtained by 2D-FFT based method (4 targets present)	8
2.3	Structure of the array and the signals impinging due to presence of a single point-scatterer, under far-field assumption	9
2.4	The so called radar data cube, representing three dimensions of radar data	12
3.1	Clutter returns	21
3.2	Simulation scene	22
3.3	Power spectral distribution of the phase noise	23
3.4	Baseband total transmitted signal	24
3.5	Positioning of elements in the array	24
3.6	Array response	25
3.7	Received signal after deramp operation	26
3.8	Magnitude of frequency response of the low-pass filter for each receiver	26
3.9	Baseband signal corresponding to one transmit-receive pair, after filtering and decimation	27
4.1	Wideband beam pattern, DoA angle vs wavelength	30
4.2	Target scene after removal of constrictions of far-field assumptions	33
4.3	The mean square error of approximation of phase shifts in consecutive elements	35
4.4	Sidelobes increase due to time varied nature of steering vectors	36
4.5	Improvement of accuracy of estimation of azimuth DoA, after using suboptimal estimates of first sweep	37
4.6	Localization of 5 randomly placed targets using 2D-MUSIC approach	38
4.7	Localization of 5 randomly placed targets using proposed method	39
5.1	Range-Azimuth spectrum, summation of all chirps	43
5.2	Range-Doppler plot, summation of all receiver elements	44
5.3	The difference of observed velocity vectors and range	44
5.4	Difference of apparent velocities between consecutive array elements	45
6.1	Effect of SNR on parameter estimation	50

6.2	Effect of sweep bandwidth on parameter estimation	51
6.3	Scatterplot of DoA estimation errors, random ranges	52
6.4	Change of azimuth error with respect to range of scatterer over multiple random experiments	53
6.5	Range-Doppler processing, 2D FFT	53
6.6	Range-Doppler processing, MUSIC	54

LIST OF TABLES

3.1	Sample values from a config structure	20
3.2	Example of a typical simulator run and parameters	21
6.1	NXP Radar Parameters	52

1

INTRODUCTION

Research on utilizing radars as comfort and safety enhancing systems on automobiles have been going on since early 1970's. Implementation of radar platforms on production vehicles have started in early 90's and since then, many different configurations and techniques have been developed to increase performance, reliability and robustness while reducing costs.

Nowadays, research and development in automotive radars is mostly divided in two, long and short range radars. Long range radars typically use the 77 GHz center frequency and have much narrower beamwidths whereas short range radars typically use the 24 GHz band and have wider scanning angle.

New developments in SiGe technology and improved signal processing algorithms allowed 77 GHz applications for automotive radars to be preferred in advanced driver assistance systems over the existing, tried and true 24 GHz systems. However, more improvement in many aspects of these systems is still open and available.

1.1. MOTIVATION

Automotive radars work in multiple moving target environments, in which it is crucial to accurately obtain positions of targets relative to the radar platform and their velocities. Imaging and range-azimuth estimation algorithms using radars have been an important area of research in automotive applications and the current research on this topic tends towards investigation of effects of wideband signals and sparse sensing using multi-channel radar systems. However, until very recently, these have ignored the movement of the targets. This research focuses on the effects of wideband LFM signals and existence of multiple, moving targets in a MIMO automotive radar setting on the existing super-resolution algorithms for estimation of range, az-

imuth angle and velocity.

1.2. RESEARCH GOALS

The main goal of this thesis is to estimate jointly three parameters of multiple targets in the scene; range, azimuth angle and radial velocity. Furthermore, it is necessary to achieve super-resolution in all three domains; that is, the algorithms provided by this thesis need to have better resolution than the limits given in chapter 2.1. For down-range estimation, this corresponds to a resolution better than what would have otherwise achieved using simple DFT based estimation on full spectrum of the bandwidth. The estimation of cross-range parameter is done by transforming the azimuth angle estimation to Cartesian coordinates with the help of down-range estimates in this context. For the purposes of super-resolution in this domain, it is necessary to surpass in accuracy the limit determined by ratio of wavelength and aperture size (in radians). Similarly, in the estimation of velocities, a resolution finer than reciprocal of the coherent pulse interval; achievable by performing DFT based spectral estimation methods over the phase shifts along the consecutive pulses.

The verification of any novel algorithm or technique will be done by comparisons of accuracy of estimations with respect to different operating parameters; comparisons with methods used in existing literature as well as theoretical bounds (Cramer-Rao bounds).

We also would like to observe the effects of wideband LFM CW waveforms on the performance and resolution in the estimation of the aforementioned parameters. Since automotive applications involve 24 GHz and 77 GHz centre frequencies, it is challenging to achieve a bandwidth that would correspond to a comparatively large fractional bandwidth; but new technologies in antenna design and MMIC design allow for such large bandwidth signals to be transmitted.

Finally, we would like to investigate the effects of the movement of the targets on the estimation problem, especially in the case when targets are close to the aperture such that the difference of distances with respect to consecutive elements as well as observed radial velocities per element cannot be ignored.

1.3. STRUCTURE AND APPROACH

The structure of the thesis work is given as follows; first a chapter (chapter 2 to be more specific) is dedicated to literature survey and problem formulation, in which the description of the estimation problem is given as well as the state-of-the-art approaches. Then a comprehensive simulator is done on MATLAB that would be able to take into account the problems described in research goals, the design steps and conclusions of which are given in chapter 3.

The first step towards problem formulation and solution is given in chapter 4, where a new signal model is derived with LFM CW automotive radars in mind, and the problem of range-azimuth estimation is tackled using the newly formed signal model.

Next, in chapter 5, the signal model is extended to include the movement of the targets, both inter- and intra- chirp effects are examined to reach the final goal of achieving super-resolution in three dimensions.

Finally, performance evaluation and comparison with respect to current trends, of the newly developed models are discussed in chapter 6. Conclusions and suggestions toward future works are given chapter 7.

2

PROBLEM FORMULATION AND LITERATURE

SURVEY

In this section, we first give a description of the problem; beginning with the principles of FMCW radar and then details of the estimation process of the three domains separately. Then we investigate the current FMCW radar super-resolution methods of joint estimation in two domains (range-azimuth and range-Doppler), particularly those that are focused on automotive applications. We analyse these methods in terms of their performance relative to external factors such as SNR, number of targets, proximity and movement of targets as well as internal factors such as transmit waveforms and bandwidth.

2.1. PROBLEM DESCRIPTION

Range-Doppler processing in FMCW radars is classically done by estimating the spectrum of the return signals from multiple continuously transmitted frequency sweeps (or chirps). In the most basic case when there is a single transmitter and a receiver, the range information can be extracted from the time samples in a single sweep and velocity information can be extracted from the phase shifts in the return signal in the same range bin over multiple pulses.

The transmit signal of an FMCW radar is given as

$$u(t) = e^{j\pi\mu t^2} \quad \text{where } \mu = \frac{\Delta F}{2T_s} \quad (2.1)$$

$$s_{LO,i}(t) = \cos(2\pi f_c t) \quad s_{LO,q}(t) = \sin(2\pi f_c t) \quad (2.2)$$

$$s(t) = s_{LO,i}(t) \operatorname{Re}\{u(t)\} - s_{LO,q}(t) \operatorname{Im}\{u(t)\} \quad (2.3)$$

Where f_c is the center frequency of the radar, ΔF is the FMCW sweep bandwidth and T_s is the sweep duration. $u(t)$ is called the complex envelope (baseband) of the signal, $s_{LO}(t)$ is the carrier signal from the local oscillator and $\operatorname{Re}\{u(t)\}$ and $\operatorname{Im}\{u(t)\}$ are the in-phase and quadrature components of $u(t)$, respectively.

Reflection of this signal from a single point scatterer results in a time shift of $\tau = \frac{2r}{c}$, where c is the speed of light in the medium. So we obtain the following signal from the receiver

$$s(t-\tau) = \operatorname{Re} \left\{ \exp \left[j2\pi \left(f_c t + \frac{\mu}{2} t^2 \right) \right] \exp \left[j2\pi \left(\frac{2r}{\lambda_c} + \frac{2\mu r}{c} t + \frac{2\mu r^2}{c^2} + \frac{2v}{\lambda_c} \cos\theta t \right) \right] \right\} \quad (2.4)$$

Here the first exponent is the transmitted signal itself, the $\frac{2r}{\lambda_c}$ term is the residual video phase, $\frac{2\mu r}{c}$ is the beat frequency, $\frac{2\mu r^2}{c^2}$ is the quadratic phase term and $\frac{2v}{\lambda_c} \cos\theta$ is the Doppler frequency. The quadratic phase term is usually ignored, due to the fact that $c \gg r$. For simplicity, we assume that the target movement is only on the axis that is perpendicular to the array plane, thus θ is the direction of arrival of the reflected signal, as well as the angle between the velocity vector of the target and radial direction towards the first element of the array, as depicted in figure 5.3. [1]

So we can see that the estimation of the range of a target is equivalent to the estimation of the beat frequency of the return signal. Resolution in range is therefore dependent on the resolution of the frequency estimation algorithm utilized in determination of the beat frequency. Using a simple FFT based method, we obtain a frequency resolution of $\frac{f_s}{N}$, where f_s is the sampling frequency and N is the number of samples (or frequency bins). This corresponds to a range resolution of $\frac{c}{2\Delta F}$. [2] Super-resolution algorithms that are discussed further in chapter 2.2 try to overcome this resolution, usually by compromises in other domains such as lost resolution in other frequency bands or computational complexity.

The movement of targets causes the reflected signal to change in frequency depending on the direction of motion relative to the antenna. The Doppler shift can be observed in the spectrogram of the reflected signal of an LFMCW waveform as in figure 2.1; the horizontal shift in the instantaneous frequency is caused by the time delay and the vertical shift is caused by the Doppler effect.

The reason why multiple pulses are used for Doppler processing is that, for most cases, the Doppler shift introduced by movement of targets is several orders of magnitude less than the bandwidth of the signal of interest. [2] This fact holds true for both pulsed radars and continuous wave radars; also for non-modulated waveforms or pulse-compressed waveforms. A special case in FMCW radars is that, since the Doppler frequency shift is present on top of the beat frequency introduced by the time shift, it's difficult to resolve velocities of multiple targets even if the Doppler frequency shift was within the frequency resolution of the spectrum estimation algorithm that is employed to find the beat frequency. For this purpose, various methods involving different types of FMCW waveforms are utilized, such as non-linear frequency modulation,

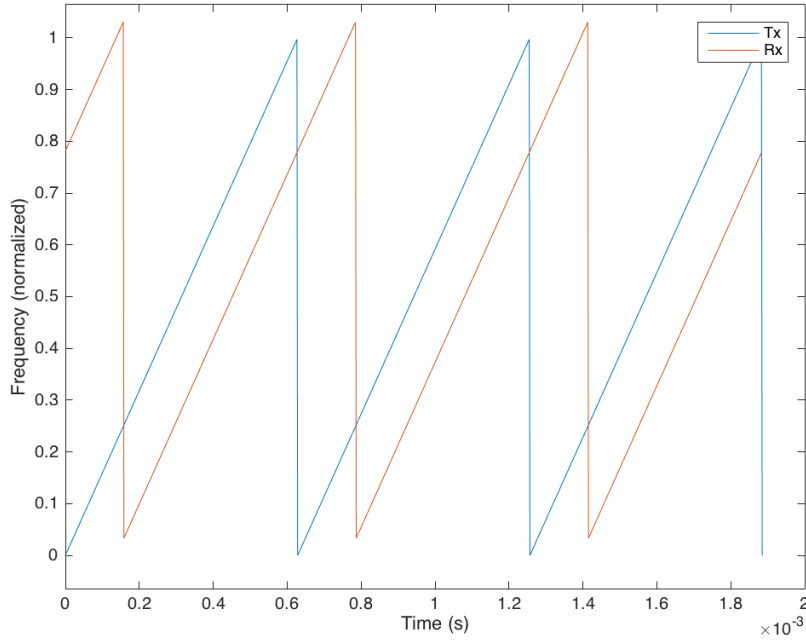


Figure 2.1: Simplified spectrum of the transmit and receive signals of LFMCW radar

stepped frequency modulation.

Using multiple sweeps, we assume that the motion of the target is linear within the sweep duration (a reasonable assumption, since sweep duration in automotive FMCW radar systems is usually in the order of 10-1000 μs). Since intra-pulse Doppler is ignored, we obtain the following signal model [3]

$$s(t) = \sum_{h=0}^{H-1} \exp \left\{ j2\pi \left[\frac{2}{\lambda_c} (r + vT_s h) + \frac{2\mu}{c} (r + vT_s h) t + \frac{2v}{\lambda_c} \cos\theta t \right] \right\} \text{rect} \left(\frac{t - hT_s}{T_s} \right) \quad (2.5)$$

Where H is the number of sweeps (depends on dwell time) and rect is the rectangular window function. Collecting each of the pulses in the rows of the array, we obtain the so called data matrix. A 2D spectrum analysis on this 2D data matrix gives us the Range-Doppler graph, as can be seen in figure 2.2. A two-dimensional Fourier transform is a widely used technique in estimation of range and velocity information of targets; for detection of targets, a CFAR algorithm can be used on the Doppler domain obtained after processing.

The velocity resolution of range-Doppler processing is given as $\frac{\lambda_c}{HT_s}$, where H is the total number of sweeps transmitted. [2]

However, information about range and velocities of multiple targets in an area is not enough for localization of the targets; there can be multiple targets in a single range bin and a target in a range bin can be anywhere on a circle with radius equal to the estimated range and the center at the position of the radar. In order to have a 2D image of the scene, we also require the azimuth angles of the targets with respect to the radar. There are multiple ways of estimation of direction of target; since radar beams are modeled as cones with certain 3 dB beamwidths, only the targets within that area give strong reflections, so steering the beams to measure data from different aspects of angle gives information of direction of the reflector. However, this

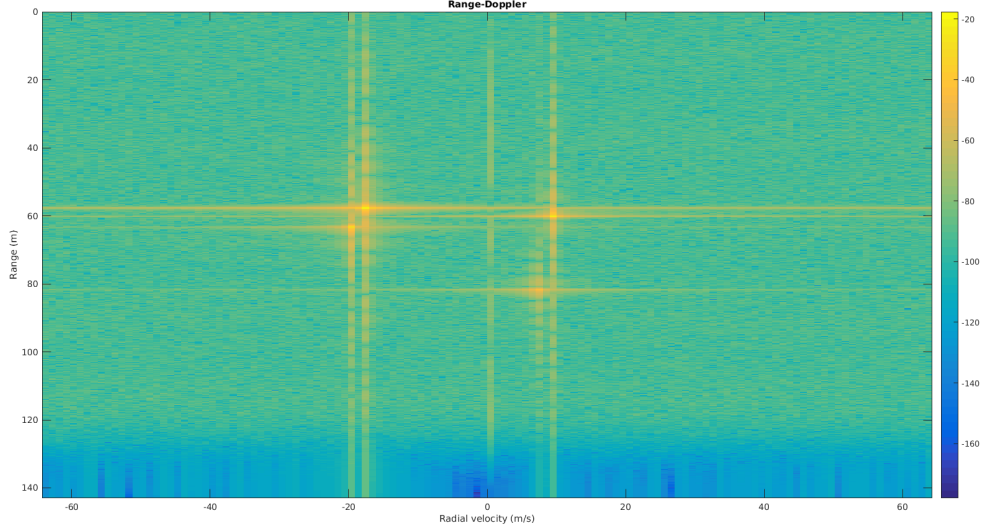


Figure 2.2: A Range-Doppler plot obtained by 2D-FFT based method (4 targets present)

work is focused on array signal processing based methods (mainly digital beamforming algorithms on MIMO arrays) for the estimation of direction of targets. Since the degrees of freedom are distributed among transmitter and receiver elements, we will use the virtual array concept and simplify MIMO systems as equivalent MISO systems and then extend the signal model and algorithms to include MIMO systems.

Having multiple elements in the virtual array means that depending on the direction of arrival of the return signal, each other element receives a delayed version of the signal that arrived first to a particular element. Under far-field assumptions, the wavefront is assumed to be planar, thus the line of sight from each element to the target can be shown as parallel and the time delays for each consecutive element is linearly increasing in a uniform linear array. As can be seen in figure 2.3, the signals travels $d \sin \theta$ distance more in each consecutive element, meaning a time delay of $\frac{d \sin \theta}{c}$. So, for a real valued bandpass signal $u(t)$ with center frequency of f_c and complex envelope $s(t)$ such that

$$u(t) = \text{real}\{s(t)e^{j2\pi f_c t}\} = x(t)\cos(2\pi f_c t) - y(t)\sin(2\pi f_c t) \quad (2.6)$$

this time delay is represented as

$$u(t - \tau) = \text{real}\{s(t - \tau)e^{j2\pi f_c (t - \tau)}\} = \text{real}\{s(t - \tau)e^{-j2\pi f_c \tau} e^{j2\pi f_c t}\} \quad (2.7)$$

Under narrowband assumption, in order to reduce the effects of time delay over the ULA to phase shifts, the following approximation is made

$$s(t - \tau) = \int_{-\Delta F/2}^{\Delta F/2} S(f)e^{-j2\pi f \tau} e^{j2\pi f t} df \approx \int_{-\Delta F/2}^{\Delta F/2} S(f)e^{j2\pi f t} df = s(t) \quad (2.8)$$

$$\text{when } |2\pi f \tau| \ll 1 \text{ for } f < \left| \frac{\Delta F}{2} \right| \text{ so } e^{-j2\pi f \tau} \approx 1 \quad (2.9)$$

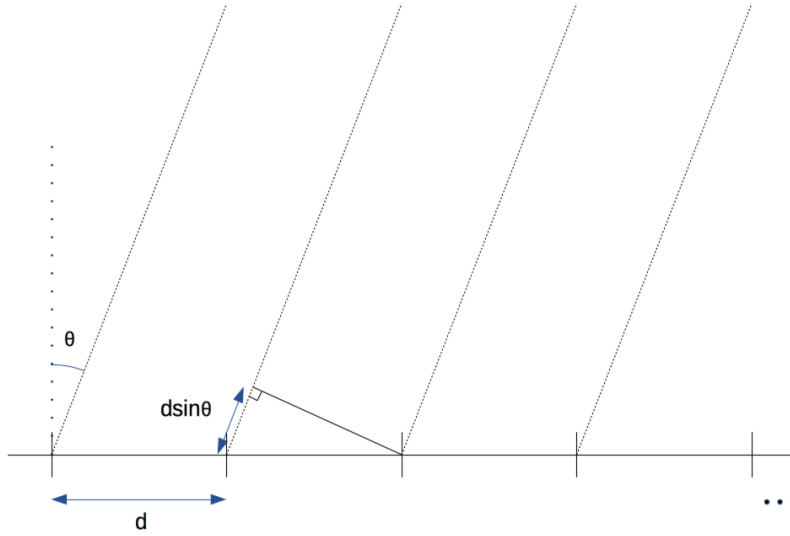


Figure 2.3: Structure of the array and the signals impinging due to presence of a single point-scatterer, under far-field assumption

So we have

$$u(t - \tau) = \text{real}\{s(t - \tau)e^{j2\pi f_c \tau} e^{j2\pi f_c t}\} = \text{real}\{s(t)e^{-j2\pi f_c \tau} e^{j2\pi f_c t}\} \quad (2.10)$$

Combining figure 2.3 and equation 2.10, for a ULA, under narrowband and far-field assumptions, we get

$$\left. \begin{aligned} x_1(t) &= u(t) \\ x_m(t) &= u(t - \tau) = u(t)e^{-j2\pi f_c m\tau} \end{aligned} \right\} a = \frac{x_m}{x_1} = e^{-j2\pi f_c m\tau} = e^{-j2\pi \frac{md}{\lambda} \sin\theta} \quad (2.11)$$

When time samples from each element is collected in a vector, it is represented as

$$\mathbf{x}(t) = \sum_{k=1}^K \gamma_k \mathbf{a}(\theta_{a,k}) s(t - \tau_k) + w(t) \quad (2.12)$$

Where γ_k is the complex scattering coefficient of target k , proportional to its RCS, $\mathbf{a}(\theta_{a,k})$ is the array response to the k^{th} target at an angle of arrival of $\theta_{a,k}$, τ_k is the delay associated with target k ($\tau_k = \frac{2r_k}{c}$) and finally $w(t)$ is the noise, assumed white Gaussian in this case.

After discretization, the signal model can be derived as

$$\mathbf{X} = \mathbf{A}\mathbf{S} + \mathbf{W} \quad (2.13)$$

Where

$$\mathbf{A} = [\mathbf{a}(\theta_{a,1}) \cdots \mathbf{a}(\theta_{a,K})] \quad (2.14)$$

$$\Gamma = \text{diag}[\gamma_1 \cdots \gamma_K] \quad (2.15)$$

$$\mathbf{S} = [s_{\tau_1} \cdots s_{\tau_K}]^T \quad (2.16)$$

And \mathbf{W} contains noise samples, modeled as complex Gaussian white noise. In the case when noise cannot be considered independent, pre-whitening filters are used.

The resolution of digital beamformer based DoA estimation methods depend on the width of the main-beam of the antenna array response. So, the more elements an array has, the less the resolution becomes. Based on the main beamwidth, for simple DBF methods, this resolution is $\frac{2\pi}{M}$. In order to achieve super-resolution, we need to get rid of the dependence of resolution to the aperture size. This is possible with subspace based methods, as explained in chapter 2.2, with the example trade-offs being increased computational complexity, additional problem of estimating number of sources and low performance in low SNR scenarios.

In MIMO systems, we need to take into account the transmit steering vector, \mathbf{b} , which takes as a parameter the direction of departure, θ_d , which is formulated in the same way as the receiver steering vector under narrowband conditions.

There are two types of MIMO radar configurations; colocated and statistical. Statistical MIMO refers to the type of radar system with widely separated antennas, like in bistatic or multistatic configuration. In this thesis, we will concentrate on colocated MIMO radars.

In order to use MIMO configuration to its full extend, the transmitted waveforms need to be linearly independent to each other. That way, N_T times more targets can be identified compared to MISO configuration, assuming transmit and receive elements of the array are different.

For the MIMO system, we instead have the following data equations. The received signal reflected from one target is given as

$$\mathbf{X} = \gamma \mathbf{a}(\theta_a) \mathbf{b}(\theta_d)^T \mathbf{S}(T) + \mathbf{W} \quad (2.17)$$

If we have a total of K targets, this becomes

$$\mathbf{X} = \sum_{k=1}^K \gamma_k \mathbf{a}(\theta_{a,k}) \mathbf{b}(\theta_{d,k})^T \mathbf{S}(R_k) + \mathbf{W} \quad (2.18)$$

We can reduce this summation to a matrix equation as follows

$$\mathbf{A} = \begin{bmatrix} \mathbf{a}(\theta_{a,1})\mathbf{b}(\theta_{d,1})^T \\ \vdots \\ \mathbf{a}(\theta_{a,K})\mathbf{b}(\theta_{d,K})^T \end{bmatrix} \quad (2.19)$$

$$\mathbf{S} = \begin{bmatrix} \mathbf{S}(R_1) \\ \vdots \\ \mathbf{S}(R_K) \end{bmatrix} \quad (2.20)$$

$$\mathbf{X} = \mathbf{A}\mathbf{\Gamma}\mathbf{S} + \mathbf{W} \quad (2.21)$$

Direction of arrival estimation methods can be divided into two main categories; parameter based estimation algorithms and spectral estimation algorithms.

The most basic array processing methods for azimuth angle degree of arrival estimation is the classical (or Bartlett) beamformer. By introducing weights w_1, w_2, \dots, w_M for each of the array elements and combining the outputs, it is possible to steer the beam towards an angle of interest. The output of this processing can be written as a simple linear combination as follows

$$x(t) = \sum_{m=1}^M s_m(t) w_m^* \quad (2.22)$$

In order to steer the main beam towards a particular direction, θ_0 , the angle response is shifted as follows

$$a_m(\theta_0) = e^{j2\pi \frac{md}{\lambda} \sin(\theta_0)} \quad (2.23)$$

Using this, we look for the angle θ that maximizes the output power of the beamformer, $P(w) = \mathbf{w}^H \mathbf{R}_x \mathbf{w}$, as follows

$$\hat{\theta} = \max_{\mathbf{w}} \frac{\mathbf{w}^H \mathbf{R}_x \mathbf{w}}{\mathbf{w}^H \mathbf{w}} \quad (2.24)$$

Where R_x is the sample covariance matrix of \mathbf{X} , defined in equation 2.13. The angular resolution of this method depends on the number of elements in the virtual array. More information about other DoA algorithms is given in chapter 2.2

However, separate investigations of range and direction of arrival is not useful, for the case when multiple targets are present, this results in a problem of data association. In order to overcome this problem, investigation of simultaneous 2D range-azimuth processing method is necessary. Details about these algorithms are given in chapter 2.2.

A further step is the simultaneous estimation of 3 parameters (range, azimuth and velocity) in 3 dimensions. The data matrix becomes a data cube when multiple transmitter and/or receiver elements are introduced to the radar system. This corresponds to addition of another dimension for the signal model; the spatial dimension. Assuming only a single point reflector exists in the area of interest, the spacing of the ele-

ments of this array causes time delays between the reception of the impinging signal, based on the angle of the incident wavefront with respect to the normal of the array.

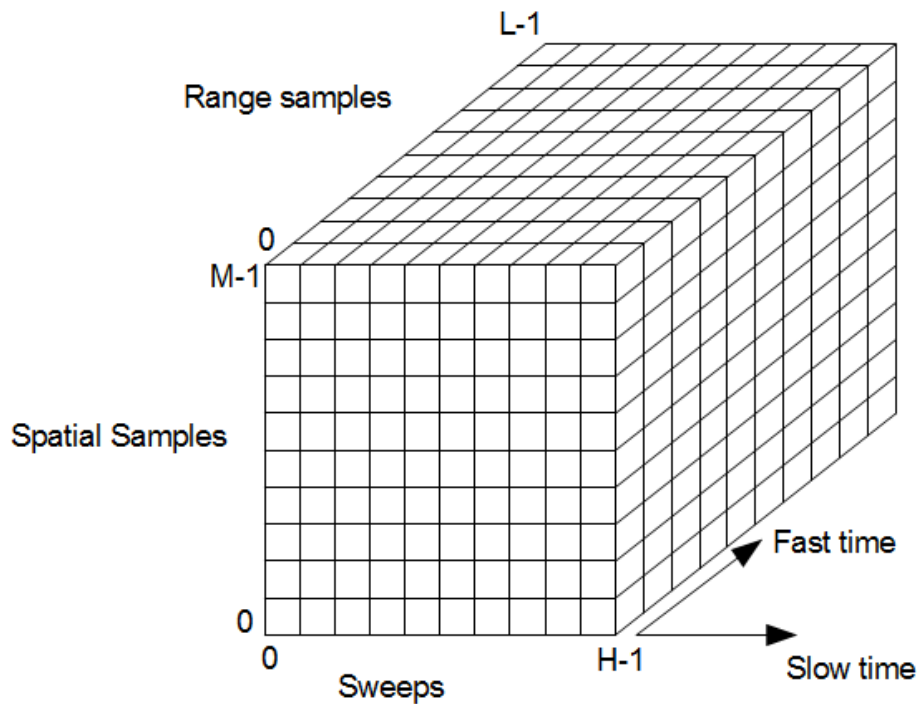


Figure 2.4: The so called radar data cube, representing three dimensions of radar data

For each dimension in this data cube, we have parameters to estimate within complex exponentials. Fast time samples contain range information in the beat frequency, slow time samples contain the velocity information in the Doppler frequency and the spatial samples contain the information of direction of arrival (azimuth angle) as phase shifts between samples.

So far, research of this problem mainly consists of estimation of two out of three of these parameters (range-Doppler or range-azimuth). For the case of range-Doppler estimation algorithms, it is more common to use 2D FFT based algorithms, limiting the resolution of both dimensions of data. For the case of range-azimuth estimation methods, the effects of increased bandwidth of transmit signals continue to be a limiting factor. The existing wideband range-azimuth estimation methods are discussed in chapter 2.2.

An additional research topic is the near-field effects on azimuth angle estimation and Doppler estimation. State of the art research on 2D range-azimuth estimation mostly ignores the movement of the target. In [4], the intra-pulse Doppler shifts are introduced to the signal model as Hadamard product and an IAA based algorithm is used in MIMO radar imaging setting. However, the near-field effects on Doppler processing in MIMO settings is not accounted for.

2.2. CURRENT APPROACHES TO DOA ESTIMATION

Several spectral estimation methods used in DoA estimation problems in array processing and MIMO communication and radar applications are given in this chapter. An overview, as well as works using these methods is discussed and finally a comparison is given.

2.2.1. MVDR (CAPON)

MVDR (or sometimes referred as Capon) beamformer is a type of data-dependent beamformer that minimizes the total output power (hence *minimum variance*) while constraining the beamformer to have fixed response towards the source (hence *distortionless*). This can be formulated as follows

$$\begin{aligned} & \underset{\mathbf{w}}{\text{minimize}} && \mathbf{w}^H \mathbf{R}_X \mathbf{w} \\ & \text{subject to} && \mathbf{w}^H \mathbf{a}_R = 1 \end{aligned} \quad (2.25)$$

The solution to this problem is given as

$$\mathbf{w} = \frac{\mathbf{R}_X^{-1} \mathbf{a}}{\mathbf{a}^H \mathbf{R}_X^{-1} \mathbf{a}} \quad (2.26)$$

With the beamformer known, we can find DoA estimates as peaks in the power spectrum given as

$$P(\theta_a) = \frac{1}{\mathbf{a}(\theta_a)^H \mathbf{R}_X^{-1} \mathbf{a}(\theta_a)} \quad (2.27)$$

In MIMO configuration, following equation 2.19, the beamformer becomes

$$\mathbf{w} = \frac{\mathbf{R}_X^{-1} \mathbf{a} \otimes \mathbf{b}}{(\mathbf{a} \otimes \mathbf{b})^H \mathbf{R}_X^{-1} \mathbf{a} \otimes \mathbf{b}} \quad (2.28)$$

And thus the power spectrum is given as

$$P(\theta_a, \theta_d) = \frac{1}{(\mathbf{a}(\theta_a) \otimes \mathbf{b}(\theta_d))^H \mathbf{R}_X^{-1} \mathbf{a}(\theta_a) \otimes \mathbf{b}(\theta_d)} \quad (2.29)$$

MVDR based beamformers have the advantage of requiring no apriori information over the scene, however, the computation of inverse of autocorrelation matrix makes these methods computationally expensive, furthermore, the performance drops significantly in low SNR situations compared to subspace based methods. MVDR based algorithms are used in [5] for localisation of emitters in low SNR conditions, as an alternative for ML based estimators and in [6], it is used for through-the-wall radar imaging in both near-field and far-field scenes as an alternative for delay-and-sum beamformers.

2.2.2. APES

The APES (Amplitude and Phase ESTimation) approach is a matched filter-bank based spectrum estimation method. It is given as the solution to the following optimization problem [7]

$$\begin{aligned} & \underset{\mathbf{h}, \alpha}{\text{minimize}} && \sum_{l=0}^L |\mathbf{h}^H \mathbf{x}(l) - \alpha e^{j\omega l}|^2 \\ & \text{subject to} && \mathbf{h}^H \mathbf{a}(\omega) = 1 \end{aligned} \quad (2.30)$$

Where the filter \mathbf{h} has order \mathbf{M} and $L = N - M + 1$. Let $\mathbf{g}(\omega) = (1/L) \sum_{l=0}^L \mathbf{x}(l) e^{-j\omega l}$ and $\hat{\mathbf{Q}} = \mathbf{R}_X - \mathbf{g}(\omega) \mathbf{g}^H(\omega)$. Then this optimization becomes

$$\begin{aligned} & \underset{\mathbf{h}}{\text{minimize}} && \mathbf{h}^H \hat{\mathbf{Q}}(\omega) \mathbf{h} \\ & \text{subject to} && \mathbf{h}^H \mathbf{a} = 1 \end{aligned} \quad (2.31)$$

The result of which gives us the APES filter as

$$\mathbf{h}_{APES} = \frac{\hat{\mathbf{Q}}^{-1}(\omega) \mathbf{a}(\omega)}{\mathbf{a}^H(\omega) \hat{\mathbf{Q}}^{-1}(\omega) \mathbf{a}(\omega)} \quad (2.32)$$

The parameter ω , whose spectrum is estimated, can be of any dimensionality. Therefore, it can be used in two ways in this application; a two dimensional temporal and spatial frequencies defined as the beat frequency and phase shift due to DoA or a one dimensional complex phase response entity, from which the DoA information can be extracted if the ToA (range) is known [8].

The comparison between APES and MVDR based spectrum estimation is given in [9], where it is found that APES has biased frequency estimation and MVDR has biased amplitude estimation, and a method combining these two is given. In [10], a similar combination method is used for multiple target localisation using MIMO radars.

2.2.3. SUBSPACE BASED METHODS

Subspace based methods use the fact that the signal space, which is composed of the reflected signals from the targets, is orthogonal to the noise subspace.

We can see from equation 2.13 that the vector of received signals $\mathbf{x}(t)$ is composed of linear combination of the columns of \mathbf{A} . These columns of \mathbf{A} are the directional mode vectors $\mathbf{a}(\theta_{a,1}) \cdots \mathbf{a}(\theta_{a,K})$ and they form a K dimensional subspace within the N_R dimensional space where all possible directional mode vectors $\mathbf{a}(\theta_a)$ (the array manifold) resides. In order to find the directions of arrival, we need to look for the intersections of the column space of \mathbf{A} to the array manifold.

The noise vectors are also present in this N_R dimensional space, but they are orthogonal to the subspace spanned by \mathbf{A} 's columns. Thus, the expression of the autocorrelation matrix of \mathbf{X} is given as

$$\mathbf{R}_X = E[\mathbf{X}\mathbf{X}^H] \quad (2.33)$$

$$= E[\mathbf{A}\mathbf{S}\mathbf{S}^H \mathbf{A}^H + \mathbf{A}\mathbf{S}\mathbf{S}^H + \mathbf{W}\mathbf{S}^H \mathbf{A}^H + \mathbf{W}\mathbf{W}^H] \quad (2.34)$$

$$= E[\mathbf{A}\mathbf{S}\mathbf{S}^H \mathbf{A}^H] + E[\mathbf{W}\mathbf{W}^H] \quad (2.35)$$

$$= \mathbf{A}\mathbf{R}_S \mathbf{A}^H + \sigma_n^2 \Sigma_{\mathbf{W}} \quad (2.36)$$

Where R_S is the autocorrelation matrix of the incident waveforms. The structure of this matrix informs us about the correlation amongst impinging signals from different targets.

Without noise, the rank of the autocorrelation matrix \mathbf{R}_X would be the number of targets, T . If $T < N_R$, we can already determine the number of targets using eigendecomposition. It is given as

$$\mathbf{R}_X = \mathbf{U}\mathbf{\Lambda}\mathbf{U}^H \quad (2.37)$$

$\mathbf{\Lambda}$ contains the eigenvalues of \mathbf{R}_X on its diagonal and since we know that rank of \mathbf{X} is T , it will have T non-zero entries and $N_R - T$ zero entries. The eigenvectors corresponding to non-zero eigenvalues are called signal eigenvectors and the ones corresponding to zeros are called noise eigenvectors. Noise eigenvectors are orthogonal to the space spanned by the columns of \mathbf{A} .

MUSIC

MUSIC (MUltiple Signal Classification) algorithm seeks for the highest Euclidean distance of all possible directional mode vectors to the noise subspace spanned by the noise eigenvectors. This distance is given as $d^2 = \mathbf{a}^H(\theta_a)\mathbf{U}_N\mathbf{U}_N^H\mathbf{a}(\theta_a)$. MUSIC grants asymptotically unbiased estimate of target DoA. The spectrum is given as

$$P(\theta_a) = \frac{1}{\mathbf{a}(\theta_a)^H\mathbf{U}_N\mathbf{U}_N^H\mathbf{a}(\theta_a)} \quad (2.38)$$

This algorithm is one of the most widely used super-resolution algorithms in MIMO or MISO automotive radars and FMCW radars in general for estimation of direction of arrival. There are several improvements over the algorithm which was first proposed in [11]. These include performance improvements such as reduced dimension MUSIC or root MUSIC.

In MIMO MUSIC, the directional mode vectors are given as $\mathbf{a}_R(\theta_a) \otimes \mathbf{a}_T(\theta_d)$, as seen in equation 2.19. Therefore, the distance between directional mode vectors and noise subspace is given as $d^2 = (\mathbf{a}_R(\theta_a) \otimes \mathbf{a}_T(\theta_d))^H\mathbf{U}_N\mathbf{U}_N^H(\mathbf{a}_R(\theta_a) \otimes \mathbf{a}_T(\theta_d))$ and thus the spectrum becomes

$$P(\theta_a, \theta_d) = \frac{1}{(\mathbf{a}(\theta_a) \otimes \mathbf{b}(\theta_d))^H\mathbf{U}_N\mathbf{U}_N^H(\mathbf{a}(\theta_a) \otimes \mathbf{b}(\theta_d))} \quad (2.39)$$

MUSIC based algorithms have been used in many localisation and imaging problems because of high resolution performance and relatively low computational complexity. In [12], a 2D-MUSIC algorithm is presented which takes advantage of 2D spatial smoothing technique and coherently estimates range and azimuth in one domain (although the computational complexity remains $O(n^2)$ for n range bins and steering vectors. In [13], a similar method is used, but instead of looking for distance of steering vectors to the noise subspace, a 2D-FFT based algorithm is used for the basis of noise subspace in order to estimate range-azimuth without apriori knowledge of number of targets.

ESPRIT

ESPRIT (Estimation of Signal Parameters using Rotational Invariance Techniques) is a parametric DoA estimation algorithm that takes advantage of the shift invariance property of the array; that the sensors occur in matched pairs with identical displacement vectors [14].

ESPRIT algorithm splits the sensors in the array into two subarrays of length N_T , with same displacement vector for each pair of sensors. The data collected in these subarrays are denoted by matrices \mathbf{X} and \mathbf{Y} , similar to equation 2.13, and since the displacement vectors are same, they can be expressed as

$$\mathbf{X} = \mathbf{A}\mathbf{S} \quad (2.40)$$

$$\mathbf{Y} = \mathbf{A}\Phi\mathbf{S} \quad (2.41)$$

where

$$\mathbf{A} = [\mathbf{a}(\theta_1), \dots, \mathbf{a}(\theta_K)], \quad \Phi = \text{diag}\{e^{j2\pi\Delta\sin(\theta_1)}, \dots, e^{j2\pi\Delta\sin(\theta_1)}\} \quad (2.42)$$

ESPRIT algorithm does not assume any structure on the array response vectors $\mathbf{a}(\theta)$, just that there is a constant phase relation, $\phi_k = e^{j2\pi\Delta\sin(\theta)}$ between each pair of elements in the subarrays.

The matrices \mathbf{X} and \mathbf{Y} are combined as follows

$$\mathbf{Z} = \begin{bmatrix} \mathbf{X} \\ \mathbf{Y} \end{bmatrix} + \mathbf{W} = \bar{\mathbf{A}}\mathbf{S} + \mathbf{W}, \quad \bar{\mathbf{A}} = \begin{bmatrix} \mathbf{A} \\ \Phi \end{bmatrix} \quad (2.43)$$

Similarly to the data model explained in 2.13, the matrix \mathbf{Z} is composed of a K dimensional signal subspace and $2N_T - K$ dimensional noise subspace which are orthogonal to each other. Furthermore, the autocorrelation matrix \mathbf{R}_Z has a similar structure to that of 2.33; $\mathbf{R}_Z = \bar{\mathbf{A}}\mathbf{R}_S\bar{\mathbf{A}}^H + \sigma^2\Sigma_W$. We can similarly extract the eigenvectors corresponding to the K dimensional signal subspace as \mathbf{U}_S , where $\text{rank}(\mathbf{U}_S) = \text{rank}(\bar{\mathbf{A}})$ and thus there exists a unique non-singular \mathbf{T} such that $\mathbf{U}_S = \bar{\mathbf{A}}\mathbf{T}$. Due to the rotational invariance structure of the data matrix, we can decompose this matrix as follows

$$\mathbf{U}_S = \begin{bmatrix} \mathbf{U}_X \\ \mathbf{U}_Y \end{bmatrix} = \begin{bmatrix} \mathbf{A}\mathbf{T} \\ \mathbf{A}\Phi\mathbf{T} \end{bmatrix} \quad (2.44)$$

Since both subarrays receive the same reflected signals, only with a phase shift, they share the same column space and thus the matrix defined as the combination of \mathbf{U}_X and \mathbf{U}_Y as $\mathbf{U}_{XY} := [\mathbf{U}_X \ \mathbf{U}_Y]$ also has rank K . Therefore, there exists a matrix \mathbf{F} of rank K such that

$$[\mathbf{U}_X \ \mathbf{U}_Y]\mathbf{F} = \mathbf{U}_X\mathbf{F}_X + \mathbf{U}_Y\mathbf{F}_Y = \mathbf{A}\mathbf{T}\mathbf{F}_X + \mathbf{A}\Phi\mathbf{T}\mathbf{F}_Y = 0 \quad (2.45)$$

\mathbf{F} is chosen to span the null-space of \mathbf{U}_{XY} . We define another matrix Ψ as $\Psi := -\mathbf{U}_X\mathbf{U}_Y^{-1}$ and plug it in

$$\mathbf{A}\mathbf{T}\Psi = \mathbf{A}\Phi\mathbf{T}\mathbf{U}_Y\mathbf{U}_Y^{-1} = \mathbf{A}\Phi\mathbf{T} \quad (2.46)$$

Which implies

$$\mathbf{T}^{-1}\Phi\mathbf{T} = \Psi \quad (2.47)$$

Since Φ is a diagonal matrix, the left hand side gives us the eigenvalue equation; columns of \mathbf{T}^{-1} give us the eigenvectors of Ψ and diagonal entries of Φ are the eigenvalues of Ψ . Since Ψ can be obtained from the data, an eigendecomposition gives us the DoA information.

The same operations can be done by calculating the SVD of \mathbf{Z} as well, as follows

$$\mathbf{Z} = \hat{\mathbf{U}}_Z \hat{\Sigma}_Z \hat{\mathbf{V}}_Z^H \quad (2.48)$$

$$\hat{\mathbf{U}}_Z = \begin{bmatrix} \hat{\mathbf{U}}_X \\ \hat{\mathbf{U}}_Y \end{bmatrix}, \quad \hat{\mathbf{U}}_X = \mathbf{A}\mathbf{T}, \quad \hat{\mathbf{U}}_Y = \mathbf{A}\Phi\mathbf{T} \quad (2.49)$$

$$\hat{\mathbf{U}}_X^\dagger := (\hat{\mathbf{U}}_X^H \hat{\mathbf{U}}_X)^{-1} \hat{\mathbf{U}}_X^H \quad (2.50)$$

$$\hat{\mathbf{U}}_X^\dagger = (\mathbf{T}^H \mathbf{A}^H \mathbf{A} \mathbf{T})^{-1} \mathbf{T}^H \mathbf{A}^H = \mathbf{T}^{-1} \mathbf{A}^\dagger \quad (2.51)$$

$$\hat{\mathbf{U}}_X^\dagger \hat{\mathbf{U}}_Y = \mathbf{T}^{-1} \Phi \mathbf{T} \quad (2.52)$$

ESPRIT based 2D direction finding algorithm is used in [15], for estimation of angle parameters using a rectangular sparse array. The problem is not that of localisation, however, the two dimensional spectral estimation nature remains.

2.3. CONCLUSIONS

We have investigated the most popular spectrum estimation methods that are used in literature, specifically for 2D radar imaging but also for source localisation in communication applications. Among these, we prefer the subspace based methods due to their performance increases as well as their robustness against low SNR situations, which is the case that is most likely observed in automotive radar applications.

By formulation of new signal models in chapters 4 and 5, are done in order to overcome the adverse effects of wideband signals and movement of targets on the estimation algorithms mentioned in this chapter. These algorithms have been implemented in radar applications for single parameter and joint range-azimuth estimations; extension of these to include Doppler effect is straightforward, and the models are given in [16], but an investigation of eigenstructure is necessary in the case of EVD based algorithms.

We choose to further investigate the 2D-MUSIC method to include the effects of moving targets as well as wideband FMCW signals, due to the fact of ease of modification of the method since it does not have any prerequisites on the array structure and target properties.

3

FMCW AUTOMOTIVE RADAR SIMULATOR

3.1. BASICS

The simulator is based on FMCW MIMO systems, utilised in traffic environment. It simulates transmitter effects such as phase noise, propagation effects such as Doppler shifts and radar range equation and receiver effects such as thermal noise. The transmit/receive array is based on colocated MIMO configuration, with monostatic elements. Furthermore, they are based on a linear array, with positions of transmit and receive antennas designed to provide better angular resolution, as will be explained in section 3.4. Everything is simulated in baseband, as simulation on 77 GHz RF is deemed too costly (computational-wise), therefore some effects such as receiver mixing cannot be represented. The physical elements, as well as constants are stored in separate structures and all the components described in the sections below are defined in functions. System parameters are stored in a config structure, and are shown in the table below. Note that these parameters are used throughout this chapter, but are subject to change and does not necessarily reflect the parameters of the system used in simulations in other chapters.

3.2. SYSTEM MODEL

In this section, we use the signal model explained in detail in section 2.1, but we need to discretize the equations. The simulations are all done on baseband, furthermore, to keep computational complexity down, we take advantage of principles of stretch processing, so the range-Doppler processing and azimuth DoA estimation are all done after deramp operations. Since the NXP Dolphin radar data is also presented in deramped

Centre frequency	77 GHz
Sweep bandwidth	1.075 GHz
Sweep duration	1.525 μ sec
Max. range	250 m
MIMO array	3 transmitters, 2 transmit subarrays 4 receivers

Table 3.1: Sample values from a config structure

form, there is no difference in estimation algorithms used on simulator data and real-life data.

The expressions below give the discretized versions of the signals dealt with:

Baseband transmitter waveform: $x_i[n] = \exp(j\pi\mu(n - (i-1)k_{max})^2)$, where $n = \frac{t}{T_s}$ and $n_{max} = \frac{T_{max}}{T_s}$

Baseband transmitter vector: $\mathbf{x}_i = [x_i[0] \ x_i[1] \ \dots \ x_i[N-1]]^T$

Transmitted signal: $x[n] = \sum_{i=1}^{N_T} x_i[n]$ and $\mathbf{x} = \sum_{i=1}^{N_T} \mathbf{x}_i$

Reflected signal impinging on receiver j : $s_j[n] = x[n - k_t]$ $t = 1, \dots, T$ and in vector form $\mathbf{s}_j = [s_j[0] \ s_j[1] \ \dots \ s_j[N-1]]^T$

Data matrix after receiver processing: $\mathbf{S} = [\mathbf{s}_{1,1} \ \mathbf{s}_{2,1} \ \dots \ \mathbf{s}_{N_T,1} \ \mathbf{s}_{1,2} \ \dots \ \mathbf{s}_{N_T,N_R}]$

3.3. ENVIRONMENT

Environment is defined by the physical constants, target placements and clutter. For this application, targets are cars or pedestrians and they are modelled as point scatterers in far-field. The target fields in the environment structure are their positions in cartesian coordinates, radial velocities, DoA and DoD's, and RCS values. The clutter reflections are simulated using the constant gamma clutter simulation of MATLAB in the phased array toolbox. This command simulates clutter returns in a homogenous environment with monostatic radar elements and free space propagation. An example of the clutter returns can be seen in figure 3.1.

The target parameters are given in the table below

3.4. TRANSMITTER

A typical hardware model for a radar simulator includes waveform generator(s), local oscillator, amplifiers and filters, quadrature upmixer and transmit antennas. Since we are dealing with a MIMO system, transmit beamformers are also included.

However, since all simulation is done on baseband in this case, we don't model the local oscillator and upmixer specifically. Therefore some effects caused by these hardware (such as nonlinearities, frequency

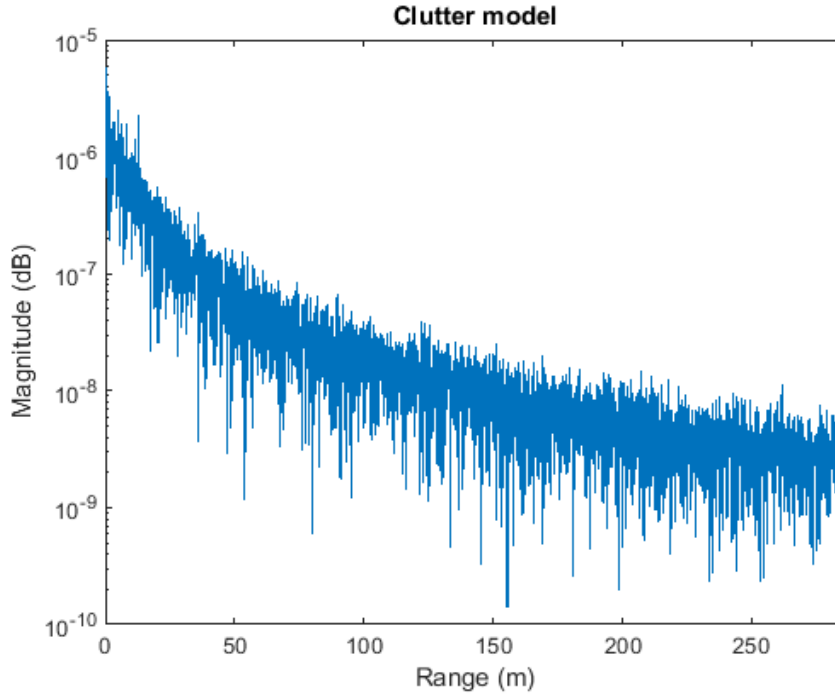


Figure 3.1: Clutter returns

	Target 1	Target 2	Target 3	Target 4	
Target Positions	21	60	30	70	m
	50	60	60	80	m
Target ranges	56.93	59.84	62.23	81.50	m
Target velocities	-17.7	8.8	-20	6.6	m/s
Target DoD	-30.6068	9.6326	-18.7139	14.2161	Degrees
Target DoA	-30.6110	9.6280	-18.7182	14.2127	Degrees
Mean RCS	100	100	100	100	m^2

Table 3.2: Example of a typical simulator run and parameters

drift etc.) are ignored. Phase noise effects are added to the final model. Phase noise is realized by Leeson's model [17], which gives the spectral distribution of single-sideband phase noise of an oscillator as follows

$$L(f_m) = 10 \log \left[\frac{1}{2} \left(\left(\frac{f_0}{2Q_1 f_m} \right)^2 + 1 \right) \left(\frac{f_{cr}}{f_m} + 1 \right) \left(\frac{FkT}{P_s} \right) \right] \quad (3.1)$$

Where f_0 is the output frequency, Q_1 is the loaded Q-factor, f_m is the offset from the output frequency, f_{cr} is the $1/f$ corner frequency, F is the noise factor of the amplifier, k is the Boltzmann constant, T is the temperature and P_s is the output power. Using MATLAB's normal distributed random generator, we obtain the following power spectrum for the phase noise

This noise is then added to the phase term of the simulated up and down mixer, separate realizations of noise for each of them.

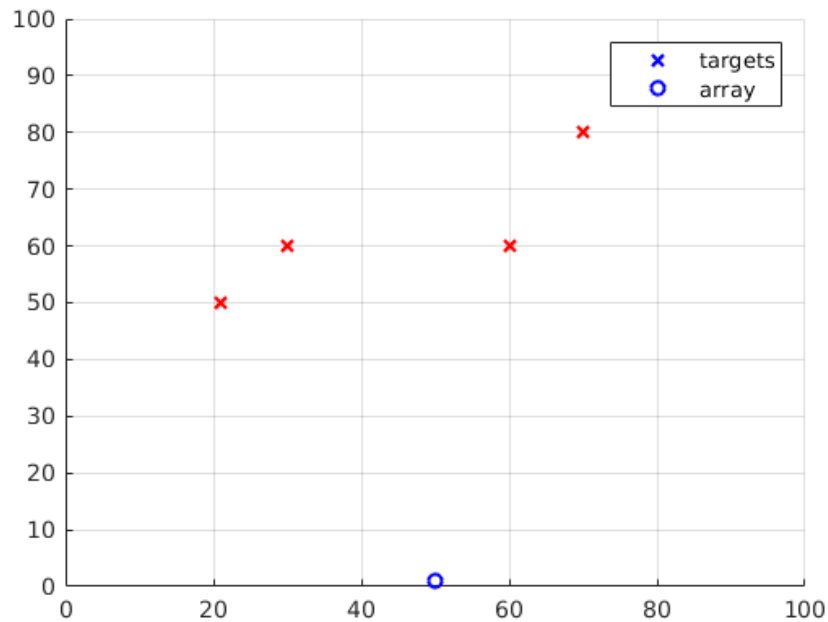


Figure 3.2: Simulation scene

To use a MIMO system to its full capacity, the choice of transmitter waveforms is crucial. For each receiver, the signals sent from each transmitter should be decoupled in order to be able to increase the elements in the virtual array [18]. To that extent, transmit waveforms should be orthogonal (or near-orthogonal) in at least one signal domain. Commonly used orthogonal transmit schemes include time domain, frequency domain and code division. A comparison of these methods, as well as others used in literature can be seen in the state of the art document.

The transmitter code makes use of the time division scheme. The generated waveform for each transmitter is linear FMCW. To be able to separate signals from each transmitter, a time delay is added for each successive transmitter. This time delay is calculated using the maximum range parameter, as follows.

$$\tau_{max} = \frac{2R_{max}}{c} \quad (3.2)$$

$$f_{shift} = \tau_{max}\mu, \quad \mu = \frac{\beta}{\tau_s} \quad (3.3)$$

Where τ_{max} is the maximum time shift, β is the sweep bandwidth and τ_s is the sweep duration. f_{shift} is the instantaneous frequency shift between successive transmissions. We can observe the orthogonality by taking a look at the signal model. The transmitted waveforms in the continuous-time model is given as

$$u_i(t) = \exp(j\pi\mu(t - (i-1)\tau_{max})^2) \quad (3.4)$$

We can stack the signals from each transmitter into a column vector as

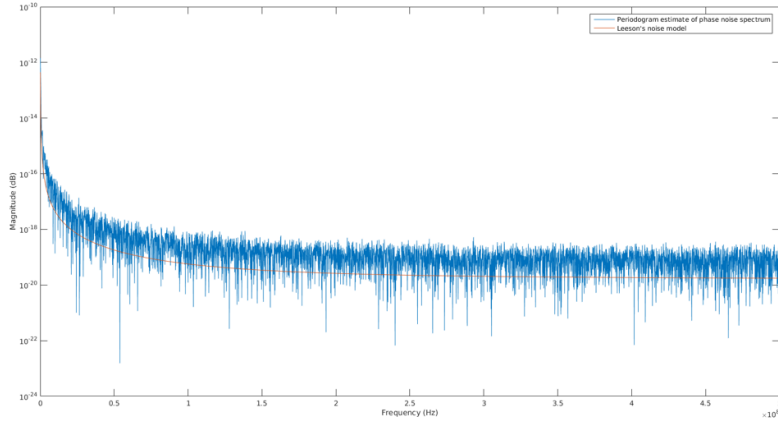


Figure 3.3: Power spectral distribution of the phase noise

$$\mathbf{u}(t) = \begin{bmatrix} u_1(t) \\ u_2(t) \\ \vdots \\ u_{N_T}(t) \end{bmatrix} \quad (3.5)$$

The correlation matrix is then given as

$$\mathbf{R}_U = \int_0^{\tau_s} \mathbf{u}(t) \mathbf{u}^H(t) dt \quad (3.6)$$

For perfect orthogonality, this matrix should be equal to identity.

If we discretize the system, we use $n = \frac{t}{T_s}$ and the equations become

$$u_i[n] = \exp(j\pi\mu(n - k_{max})^2), \quad k_{max} = \frac{\tau_{max}}{T_s}, \quad \text{where } T_s \text{ is the sample period} \quad (3.7)$$

These vectors are then stacked to form the transmit data matrix, \mathbf{X} .

A key point in designing the time division signals is that the maximum time shift times $N_T - 1$ where N_T is the number of transmitters in the array, is less than the total sweep duration (or sweep repetition interval, when it's not equal to the sweep duration). In other words, $\tau_{max} \leq (N - 1)\tau_s$. If this condition is not satisfied, one or more transmissions can be delayed into the following sweep duration, thus making all the next sweeps not orthogonal.

The spectrogram of an example transmission is given below

The MIMO utilized is linear, but not of uniform spacing. For better angular resolution, an array configuration proposed in [12] is used, where the nulls of the transmit array is used to suppress the grating lobes of the receive array. An example of such an array can be seen in

The angular response of this array can be seen below

The MIMO array response is given as

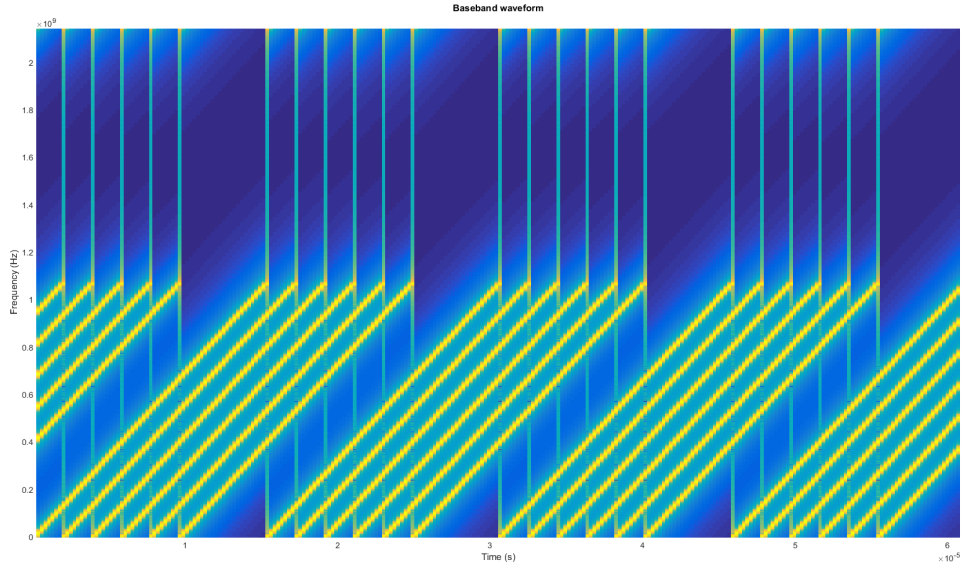


Figure 3.4: Baseband total transmitted signal

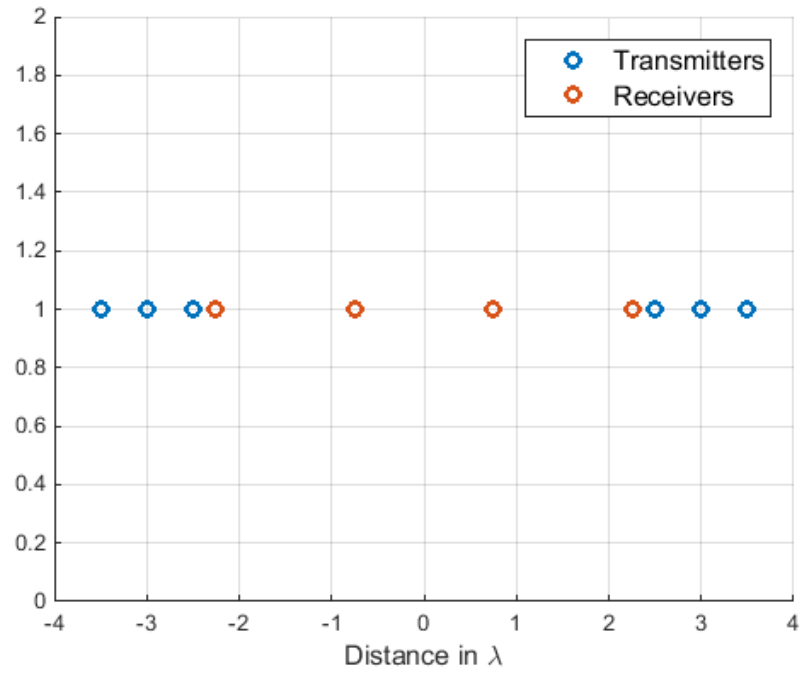


Figure 3.5: Positioning of elements in the array

$$\mathbf{a} = [1 \ e^{j\frac{2\pi}{\lambda}d_r \sin(\theta_a)} \ e^{j\frac{2\pi}{\lambda}2d_r \sin(\theta_a)} \ \dots \ e^{j\frac{2\pi}{\lambda}(N_R-1)d_r \sin(\theta_a)}]^T \quad (3.8)$$

$$\mathbf{b} = [1 \ \dots \ e^{j\frac{2\pi}{\lambda}(m_{tx}-1)D_t \sin(\theta_a)}] \otimes [1 \ \dots \ e^{j\frac{2\pi}{\lambda}(n_{tx}-1)d_t \sin(\theta_a)}]^T \quad (3.9)$$

$$\mathbf{A} = \mathbf{ab}^T \quad (3.10)$$

$$(3.11)$$

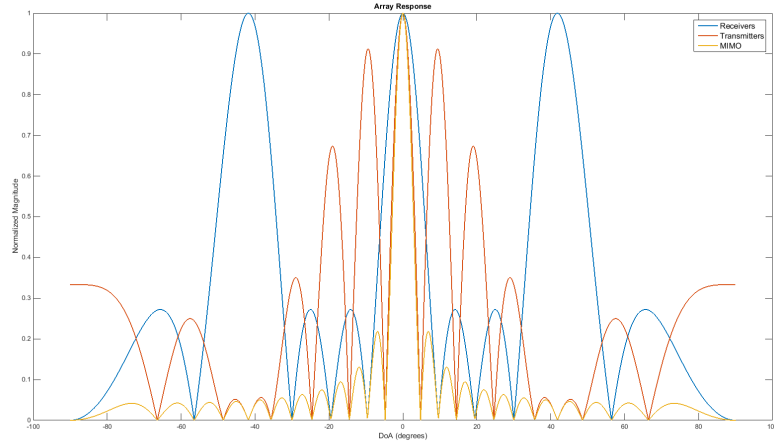


Figure 3.6: Array response

3.5. RECEIVER

Each receive antenna has copies of the transmitted signals for deramp process. After this operation, we are left a data matrix containing copies of the received signal vector filtered with corresponding transmit waveform. Ignoring, noise, clutter and other effects, the reflected baseband signal for each receiver is in the following form

$$x_j(t) = \alpha_j \sum_{t=1}^T \sum_{m=0}^{N_T-1} \beta_m \exp(j\pi\mu[t - m\tau_{max} - \tau_t]^2), \quad j = 1, \dots, N_R \quad (3.12)$$

Where K is the number of targets, $\alpha_{r,i}$ and $\alpha_{t,m}$ are receive and transmit gain factor for i^{th} and m^{th} element, respectively, N_T is the total number of transmit elements, $m\tau_{max}$ is the time delay associated with m^{th} transmit element and τ_k is the time delay associated with k^{th} target.

We can see that the beat frequencies caused by target reflections are shifted over the spectrum by $frac{\mu\tau_{max}2}{2}$ and copied for each transmitter. This effect can be seen in figure 3.7.

Then, N_T copies of this signal is first deramped with each transmitter waveform, low-pass filtered and decimated to generate the data matrix containing each transmit-receive pair signal.

$$x'_{i,j}(t) = x_j(t)\bar{u}_i(t) \quad (3.13)$$

$$x'_{i,j}(t) = \alpha_j \sum_{t=1}^T \sum_{m=0}^{N_T-1} \beta_m \exp(j\pi\mu[t - m\tau_{max} - \tau_t]^2) \exp(-j\pi[t - i\tau_{max}]) \quad (3.14)$$

$$= \alpha_j \sum_{t=1}^T \sum_{m=0}^{N_T-1} \beta_m \exp(-j\pi\mu[2t(m-i)\tau_{max} + 2t\tau_t + 2m\tau_{max}\tau_t - (m^2 - i^2)\tau_{max}^2 - \tau_t^2]) \quad (3.15)$$

We can see that after this process, the chirp frequency is removed and all beat frequencies caused by reflections are shifted by $\frac{\mu\tau_{max}}{2}$. After this, a low-pass filter is applied for each transmit-receive pair signal to remove the repeated signals. The frequency response of a sample filter can be seen in figure 3.8

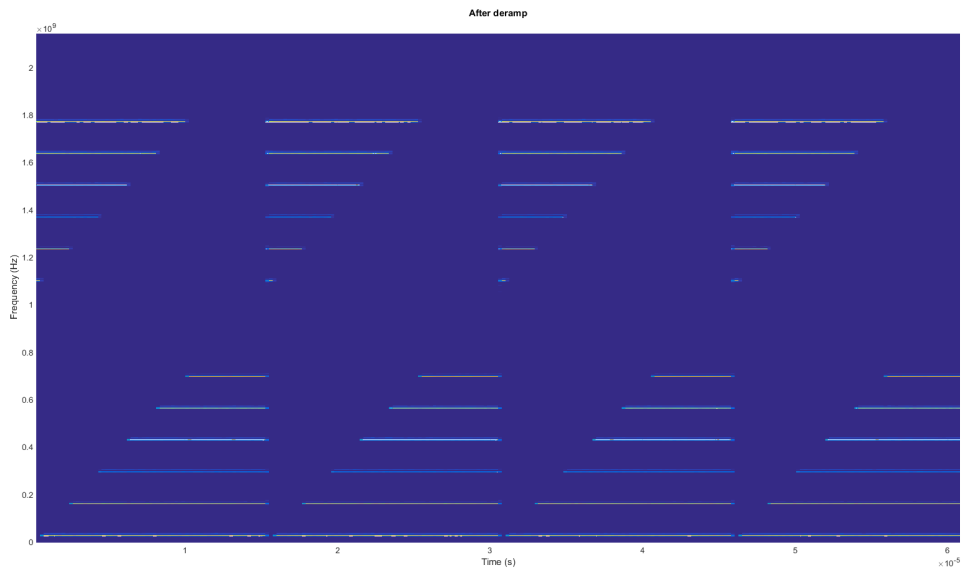


Figure 3.7: Received signal after deramp operation

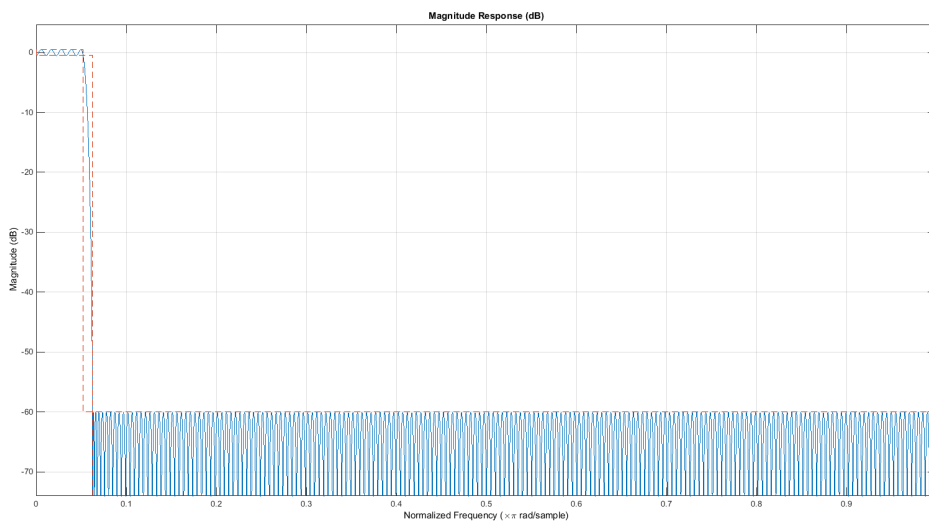


Figure 3.8: Magnitude of frequency response of the low-pass filter for each receiver

After low-pass filtering, a decimation process takes place. Range-Doppler processing and DoA estimation steps are not done on the full spectrum, as it would be too computationally complex, and also sampling the full bandwidth would not be a realistic model.

After receiver processing, the received data matrix is formed by stacking the extracted transmit-receive pair vectors.

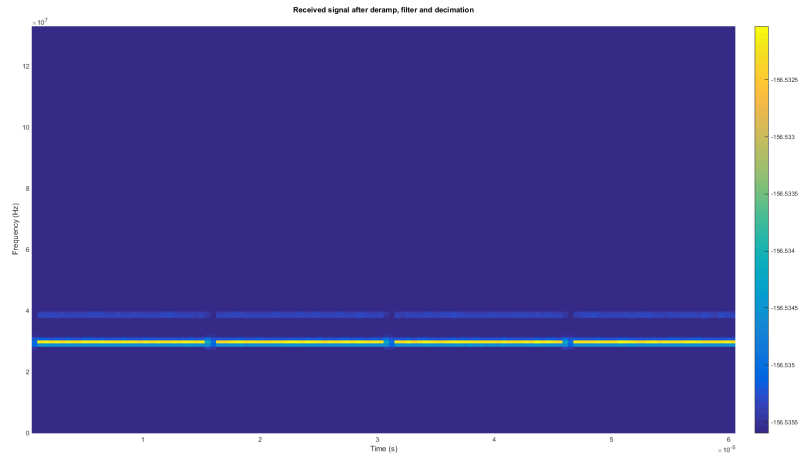


Figure 3.9: Baseband signal corresponding to one transmit-receive pair, after filtering and decimation

$$\mathbf{R} = \begin{bmatrix} \mathbf{x}_{1,1} \\ \mathbf{x}_{2,1} \\ \vdots \\ \mathbf{x}_{N_R, N_T} \end{bmatrix} \quad (3.16)$$

For simpler expressions, this output matrix is given as the output of a system with an equivalent extended virtual array in the following chapters. However, the data is still processed according to the documentation given in this chapter.

3.6. CONCLUSIONS

We provide a radar simulator in a co-located MIMO setting, taking into account details such as road clutter, transmitter and receiver thermal and phase noise effects and radar range equation. However, only point targets are considered, more complex target models are deemed to be not essential to the project goals described in chapter 1.2.

4

TARGET LOCALIZATION USING WIDEBAND LFMCW SIGNALS

Early array processing techniques for DoA estimation depended on the narrowband assumptions explained in chapter 2.1. These beamformers have significant degradation in performance when the signals of interest are not sinusoidal or narrowband. Beamformers work on the principle that for K given signals present, the contributions of $K - 1$ of them are nullified to recover the signal of interest in an environment consisting of linear combination of signals and noise. This equates to solution of a linear system as follows

$$\mathbf{X} = \mathbf{a}(\theta_1)\mathbf{x}_1^T + \mathbf{a}(\theta_2)\mathbf{x}_2^T + \cdots + \mathbf{a}(\theta_K)\mathbf{x}_K^T = \mathbf{A}\mathbf{S} \quad (4.1)$$

$$\mathbf{w}_i^H \mathbf{x}_j = \begin{cases} 1, & \text{if } i = j \\ 0, & \text{if } i \neq j \end{cases} \quad (4.2)$$

$$\mathbf{W} = [\mathbf{w}_1 \cdots \mathbf{w}_K] \quad \mathbf{W}^H \mathbf{X} = \mathbf{I} \quad (4.3)$$

It is clear that as long as \mathbf{X} is full-rank, we have a solution for \mathbf{w} . However, the array responses $\mathbf{a}(\theta_i)$ contain phase shifts corresponding to only a single frequency. Wideband signals consists of infinite number of different frequency components (complex exponentials), so it is impossible to find a beamformer that satisfies the equations above for wideband signals.

In order to visualize this problem, we can take a look at the effects of having infinitely many frequency components on the array pattern. We can see the change in array pattern in figure 4.1, where the frequency is linearly increased from 77 GHz to 85 GHz.

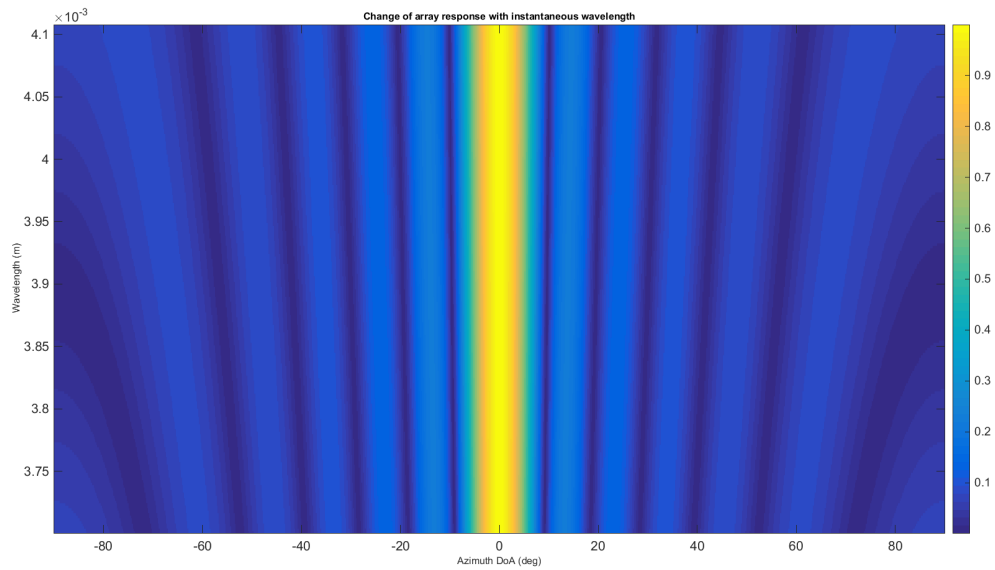


Figure 4.1: Wideband beampattern, DoA angle vs wavelength

It is clear that even though the physical size of the array is fixed, the electrical size varies with frequency. This results in wider sidelobes and thus a decrease in resolution.

As described in chapter 2.2, there are some methods for dealing with the negative effects of wideband signals. The most basic wideband beamformers utilize frequency dependent weights for a sum-and-delay beamformer approach. These frequency dependent weights can be realized as tapped delay-lines (TDL) or FIR/IIR filters. The angle and frequency dependent array response on MISO array with $J - 1$ delay-lines can be expressed as

$$x(t) = \sum_{m=0}^{M-1} \sum_{i=0}^{J-1} s_m(t - iT_s) w_{m,i}^* \quad (4.4)$$

The weights for these beamformers can be adaptively found by using various optimization algorithms. Another approach is to have array topologies that try to cover for different sub-bands of the spectrum by having non uniform placements or nested arrays.

However, these methods do not take advantage of a priori knowledge of transmitted signals. Since we are dealing with LFMCW radar, we propose a novel algorithm in which time dependent steering vectors are introduced to make it possible to include the multiple frequency components in the array pattern. The unique feature of LFMCW waveforms is the linear time dependency of the instantaneous phase of the signal and time. We exploit this feature in order to improve the angle resolution of DoA estimation methods.

4.1. JOINT DELAY-ANGLE ESTIMATION

Joint estimation of range and azimuth values in FMCW radars is a problem that can be generalized as joint angle-frequency estimation. As described in chapter 2.1, the 2D data matrix consisting of temporal and spa-

tial samples contain phase shifts and sinusoidal signals containing range information in the form of beat frequency. This data matrix is constructed by the combination of reflections from all targets as follows

$$\mathbf{X}_{n,m} = \sum_{k=1}^K \gamma_k e^{j2\pi \frac{2\mu}{c} r_k \frac{m}{f_s}} e^{j \frac{2\pi}{\lambda_c} m d \sin \theta_k} + w_{n,m} \quad (4.5)$$

In order to reduce this estimation problem to a single eigenvalue problem, we rearrange this 2D data matrix into a vector as follows

$$\mathbf{x} = [\mathbf{X}(1 \cdots L, 1) \mathbf{X}(1 \cdots L, 2) \cdots \mathbf{X}(1 \cdots L, M)]^T \quad (4.6)$$

Now, for the classical digital beamformer (Bartlett beamformer), the problem of the estimation becomes a problem of maximization of the output power, similar to that in equation 2.24, as follows

$$\{\hat{\theta}, \hat{r}\} = \underset{\mathbf{a}(\theta, r)}{\text{arg max}} \|\mathbf{a}^H \mathbf{x}\|^2 = \mathbf{a}^H \mathbf{R}_x \mathbf{a} \quad (4.7)$$

Where the steering vectors $\mathbf{a}(\theta, r)$ are given as follows

$$\mathbf{a}_r = [1 e^{j2\pi \frac{2\mu}{c} r \frac{1}{f_s}} e^{j2\pi \frac{2\mu}{c} r \frac{2}{f_s}} \cdots e^{j2\pi \frac{2\mu}{c} r \frac{L-1}{f_s}}]^T \quad (4.8)$$

$$\mathbf{a}_\theta = [1 e^{j \frac{2\pi}{\lambda_c} \sin \theta} e^{j \frac{2\pi}{\lambda_c} 2 \sin \theta} \cdots e^{j \frac{2\pi}{\lambda_c} (M-1) \sin \theta}]^T \quad (4.9)$$

$$\mathbf{a} = \mathbf{a}_\theta \otimes \mathbf{a}_r \quad (4.10)$$

In order to use MUSIC in joint estimation problem, we check the structure of the spatio-temporal auto-correlation matrix, similar as in the single parameter estimation case. Firstly, we see that since ULA's exhibit the centro-symmetry property [19], forward-backward spatial smoothing methods are widely used in order to improve detectability and combat the effects of correlation in return signals. The spatio-temporal autocorrelation matrix is given as

$$\mathbf{R}_x = \frac{1}{2p_1 p_2} \left[\sum_{m=0}^{M-m_1} \sum_{l=0}^{L-m_2} \mathbf{b}_{m,l} \mathbf{b}_{m,l}^H + \mathbf{J} \left(\sum_{m=0}^{M-m_1} \sum_{l=0}^{L-m_2} \mathbf{b}_{m,l} \mathbf{b}_{m,l}^H \right) \mathbf{J} \right] \quad (4.11)$$

Where $p_1 = M - m_1 + 1$, $p_2 = L - m_2 + 1$, m_1 and m_2 are parameters chosen such that $m_1 m_2 > 2p_1 p_2$ and $m_1 m_2 > 2L$, \mathbf{J} is a matrix with 1's on its anti-diagonal and 0's everywhere. Moreover, $\mathbf{b}_{m,l}$ is given as

$$\mathbf{b}_{m,l} = \begin{bmatrix} \mathbf{X}(l, m) \\ \vdots \\ \mathbf{X}(l + m_1 - 1, m) \\ \mathbf{X}(l, m + 1) \\ \vdots \\ \mathbf{X}(l + m_1 - 1, m + 1) \\ \vdots \\ \mathbf{X}(l + m_1 - 1, m + m_2 - 1) \end{bmatrix} \quad (4.12)$$

The reason we employ the FB-SS method is that one of the problems deteriorating the performance of eigenstructure based methods (such as MUSIC or ESPRIT) in DoA estimation is the high correlation of received signals. In radar applications, due to factors such as multipath propagation, the reflected signals are highly correlated [20] which causes the autocorrelation matrix of the incident waveforms, R_s in 2.33 to be nondiagonal but remain nonsingular. The rank of R_X decreases with each coherent wavefronts. In order to overcome this problem, a combination of spatial smoothing and forward-backward spatial smoothing algorithms have been utilised in DoA estimation algorithms involving radars.

Spatial smoothing algorithm proposed by [20] divides the ULA into overlapping subarrays of length m_1 , which makes the signal autocorrelation matrix R_S nonsingular, regardless of the coherence of the signals. Along with forward-backward spatial smoothing, this technique is akin to windowing in spatial and temporal domains, with window dimension of $m_1 \times m_2$, granting $p_1 = M - m_1 + 1$ positions in the spatial domain and $p_2 = L - m_2 + 1$ in the temporal domain [21]. As long as $m_1 m_2 > 2p_1 p_2$ and $m_1 m_2 > 2L$, the eigenstructure of the new autocorrelation matrix is the same as the old one. However, the usage of overlapping subarrays decreases the effective aperture size. But as a side benefit, the computational cost of determining the subspaces via SVD and the power spectrum decreases significantly.

Eigenstructure of this autocorrelation matrix can be examined in detail by the following factorization model [22] using the transformation matrix \mathbf{T}

$$\mathbf{R}_x = \mathbf{P}\mathbf{R}\mathbf{P}^T \times \mathbf{T} \quad (4.13)$$

The matrix \mathbf{P} contains in its columns the exponentials with delay and angle influenced terms, containing information of range and azimuth angle respectively, similar to equation 4.5, but with parameters p_1 and p_2 instead of M and L . Performing EVD on this autocorrelation matrix, assuming AWGN as usual, we see

$$\mathbf{R}_x = \mathbf{U}_x \Lambda_x \mathbf{U}_x^H + \sigma^2 \mathbf{I} \quad (4.14)$$

where we have eigenvectors spanning the signal subspace (contribution of \mathbf{U}_x) and the noise subspace (contribution of $\sigma^2 \mathbf{I}$) in the summation; similar to that of the spatial autocorrelation matrix. We isolate the eigenvectors spanning the noise subspace by choosing the eigenvectors corresponding to smaller eigenvalues (proportional to σ^2) with multiplicity $M - T$.

The space-time steering vectors in this vectorized format is given as

$$\begin{aligned} \mathbf{a}(\theta, r) = & \begin{bmatrix} 1 & \exp\left(j2\pi \frac{2\mu}{c} r \frac{1}{p_2}\right) & \cdots & \exp\left(j2\pi \frac{2\mu}{c} r \frac{p_2-1}{p_2}\right) \end{bmatrix} \\ & \otimes \begin{bmatrix} 1 & \exp\left(j \frac{2\pi}{\lambda_c} \sin(\theta) \frac{1}{p_1}\right) & \cdots & \exp\left(j \frac{2\pi}{\lambda_c} \sin(\theta) \frac{p_1-1}{p_1}\right) \end{bmatrix} \end{aligned} \quad (4.15)$$

where the second exponential term containing delay terms is for the virtual array; for a MIMO array, we simply write it as

$$\mathbf{a}_\theta = \text{vec}(\mathbf{a}\mathbf{b}) = \mathbf{a} \otimes \mathbf{b} \quad (4.16)$$

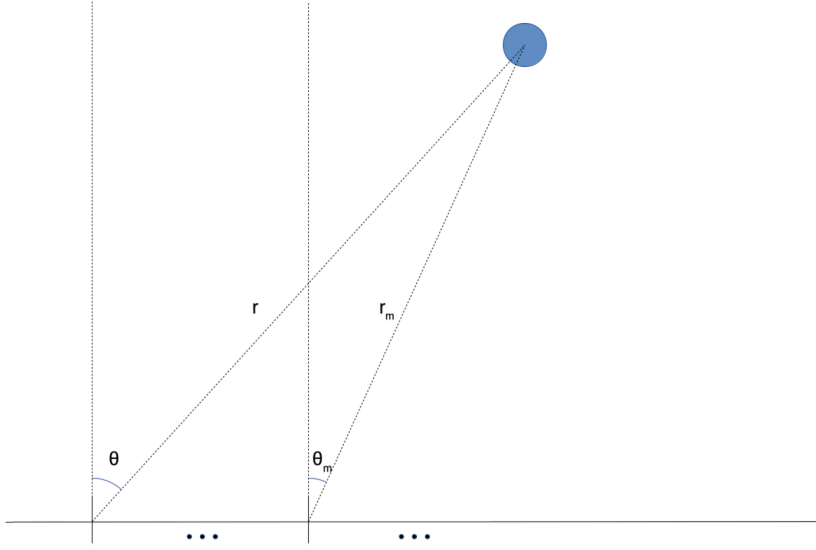


Figure 4.2: Target scene after removal of constraints of far-field assumptions

Estimation of the spectrum of beat frequencies and phase shifts can be accomplished by observing the local maxima of the cost function of MUSIC algorithm, also described as the distance of space-time steering vectors to the noise subspace, which is perpendicular to the signal subspace. This function is given below

$$P(\theta, r) = \frac{1}{\mathbf{a}(\theta, r)^H \mathbf{U}_N \mathbf{U}_N^H \mathbf{a}(\theta, r)} \quad (4.17)$$

Where \mathbf{U}_N is the portion of the data correlation matrix that spans the noise subspace, obtained similarly to 2.38, as follows

$$\mathbf{U} = \frac{1}{ML} \mathbf{xx}^H \quad (4.18)$$

$$\mathbf{U}_N = [\mathbf{U}(1 \cdots ML, 1) \mathbf{U}(1 \cdots ML, 2) \cdots \mathbf{U}(1 \cdots ML, ML - K)] \quad (4.19)$$

4.2. NEW SIGNAL MODEL

We derive a new signal model and a new expression for the array pattern based on the LFM CW waveform. We use the time division orthogonal FMCW signals as defined in chapter 3. For simplicity, the model is explained first in the virtual array setting and then expanded to the MIMO case.

The scatterers in this scenario not considered to follow the far-field assumptions, thus we don't assume plane waves and parallel line of sights for elements in the virtual array. The scenario is explained in the following figure

Assuming only a single backscatterer is present in the area, with range r_1 and azimuth angle of θ_1 the return signal is as follows

$$x_1(t) = \exp \left[j2\pi \left(f_c t + \frac{\mu}{2} t^2 \right) \right] \exp \left[-j2\pi (f_c \tau_1 + \mu \tau_1 t) \right] \exp \left[j2\pi \frac{\mu}{2} \tau_1^2 \right] \quad (4.20)$$

Replacing $\tau = \frac{2r}{c}$ and ignoring the quadratic phase term, we get

$$x_1(t) = \exp \left[j2\pi \left(f_c t + \frac{\mu}{2} t^2 \right) \right] \exp \left[j2\pi \left(\frac{2r}{\lambda_c} + \frac{2\mu}{c} r t \right) \right] \quad (4.21)$$

The first exponent is removed when downconversion and de-ramping is applied. So we are left with

$$x_1(t) = \exp \left[j2\pi \left(\frac{2r_1}{\lambda_c} + \frac{2\mu}{c} r_1 t \right) \right] \quad (4.22)$$

The m -th element in the virtual element, after downconversion and de-ramping operations, receives the following signal

$$x_m(t) = \exp \left[j2\pi \left(\frac{2r_m}{\lambda_c} + \frac{2\mu}{c} r_m t \right) \right] \quad (4.23)$$

We know that we are working with a uniform linear array, with element spacing of d , so we need to find a relation between the time difference of arrival of wavefronts of the impinging signal to the first and m -th element of the array, that is expressed in difference of instantaneous phase and is linear with respect to m . To do that, we simply observe

$$\alpha_m(t) = \frac{s_m(t)}{s_1(t)} = \frac{e^{j\pi \left[2\frac{\mu}{c} r_m t + \frac{2r_m}{\lambda_c} \right]}}{e^{j\pi \left[2\frac{\mu}{c} r_1 t + \frac{2r_1}{\lambda_c} \right]}} \quad (4.24)$$

$$= e^{j2\pi \left[\frac{\mu}{c} (r_m - r_1) t + \frac{r_m - r_1}{\lambda_c} \right]} \quad (4.25)$$

For simplicity, we substitute r as r_1 . We need to be able to define $\alpha_m(t)$ using only θ , r ; terms we want to estimate and m . To that end, we observe

$$r_m - r = \sqrt{r^2 \cos^2 \theta + (r \sin \theta + md)^2} - r = r \sqrt{1 + \frac{2md}{r} \sin \theta + \frac{m^2 d^2}{r^2}} - r \quad (4.26)$$

For purposes of linearisation, quadratic terms such as $\frac{m^2 d^2}{r^2}$ are ignored, on the basis that $r^2 \gg m^2 d^2$. Following this, we are left with

$$r_m - r \approx r \sqrt{1 + \frac{2md}{r} \sin \theta} - r \quad (4.27)$$

We expand the square root operation using Taylor series as follows

$$(1+x)^n = \sum_{k=0}^{\infty} (x)^k \binom{n}{k} \quad \text{for } |x| < 1 \quad (4.28)$$

$$\left(1 + \frac{2md}{r} \sin \theta \right)^{1/2} = 1 + \frac{md}{r} \sin \theta - \frac{m^2 d^2}{4r^2} \sin^2 \theta \dots \quad (4.29)$$

When higher order terms are ignored, we end up with a time-dependent array response whose phase and frequency terms are linear in m , as follows

$$r_m - r \approx r \sqrt{1 + \frac{2md}{r} \sin\theta} - r \approx m d \sin\theta \quad (4.30)$$

$$\alpha_m(t) = \frac{s_m(t)}{s_1(t)} = \exp\left(j\pi \left[\frac{2\mu}{c} m d \sin\theta t + \frac{2}{\lambda} m d \sin\theta \right]\right) \quad (4.31)$$

We observe the term $\frac{2}{\lambda} m d \sin\theta$ appears in the approximation, which is the antenna array response under narrowband assumptions, which does not depend on time. The term $\frac{2\mu}{c} m d \sin\theta$ changes the array response based on the instantaneous frequency of the transmit signal.

In order to confirm the validity of this approximation, we look at the minimum mean square error of the instantaneous phase shifts between two consecutive elements of an array, first determined by calculating the time difference of arrival of signals at each sampled point in space, and then calculated by equation 5.18, again for each r and θ values.

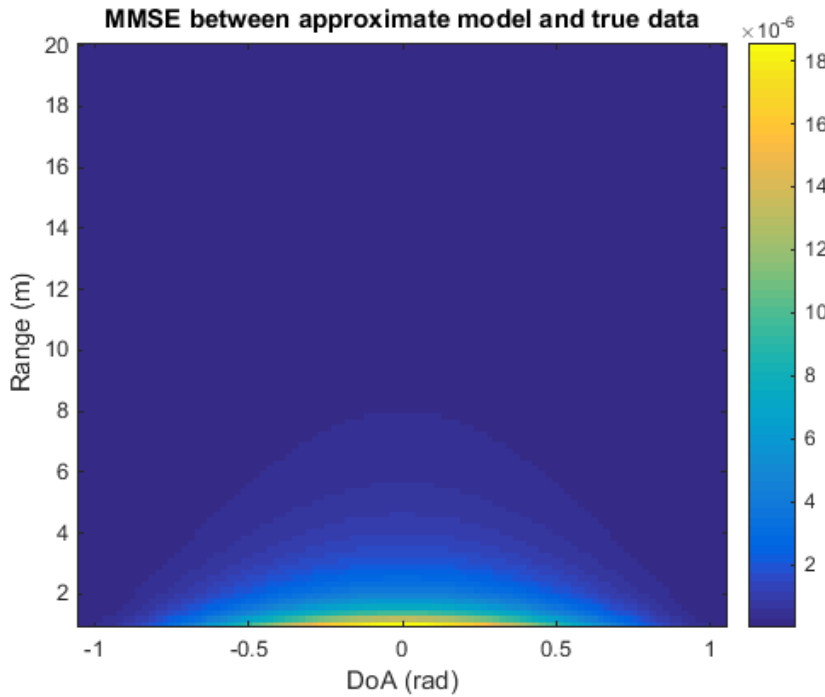


Figure 4.3: The mean square error of approximation of phase shifts in consecutive elements

As expected, the error becomes larger when objects are closer and also when θ is smaller. The prior can be explained by the fact that ignoring the higher order terms are less valid as r gets closer in value to d , and the later can be explained by the fact that $\cos\theta$ gets larger as θ gets smaller.

Since we established time varying steering vectors, it is no longer possible to represent array response in a single vector. A new signal model needs to be formulated for the specific case of LFM CW radars and multiple moving targets in close proximity. We first describe the new steering array, as follows

$$\alpha_{m,k}[n] = \exp \left[-j2\pi \left(\frac{\mu}{c} d m \sin \theta_k \frac{n}{f_s} - \frac{m d}{\lambda_c} \sin \theta_k \right) \right] \quad (4.32)$$

$$\mathbf{A}_k = \begin{bmatrix} \alpha_{1,k}[0] & \cdots & \alpha_{1,k}[L-1] \\ \vdots & & \vdots \\ \alpha_{M,k}[0] & \cdots & \alpha_{M,k}[L-1] \end{bmatrix} \quad (4.33)$$

$$\mathbf{X} = \sum_{k=1}^K \mathbf{A}_k \odot (\gamma_k \mathbf{1}_M^T \mathbf{s}_k) + \mathbf{W} \quad (4.34)$$

Where $k = 1 \cdots K$ is the target index, $m = 1 \cdots M$ is the index of the element in the virtual array and $n = 0 \cdots L - 1$ is the time sample within the sweep. \mathbf{W} is the white Gaussian noise matrix.

Now that the effects of changes in instantaneous frequency (conversely wavelength) is not ignored, the steering vectors become time dependent and we see changes in the array response with time. We can see the increase of sidelobes due to change in wavelength, in figure 4.4 below.

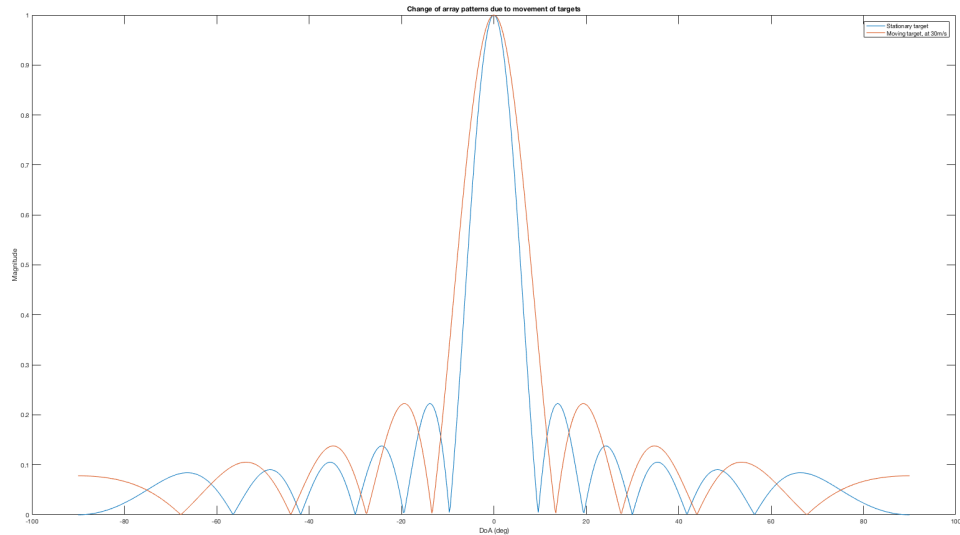


Figure 4.4: Sidelobes increase due to time varied nature of steering vectors

We can observe the negative effects of ignoring wideband nature of the transmitted signals as a decrease in resolution caused by increased main-lobe width and sidelobes.

4.3. PROPOSED METHODS

To mitigate the detrimental effects the increased bandwidth of the transmit signals on resolution and accuracy of estimation of range and azimuth DoA parameters, we propose the following two methods: first based on phase compensation and the second based on modification of steering vectors.

4.3.1. PHASE COMPENSATION OF MOVEMENT OF TARGETS IN SUBSEQUENT SWEEPS

A straightforward way of dealing with the aforementioned performance degradation problems is to remove the time dependent terms on the spatial samples of the impinging signals. This can be done by a sub-optimal estimation of the parameters r and θ for the target and then using those estimations to compensate; as follows

$$\{\hat{\theta}, \hat{r}\} = \underset{\theta, r}{\operatorname{argmax}} |P(\theta, r)| \quad (4.35)$$

$$\alpha_{comp,m}(t) = \alpha(-t) = e^{-j2\pi\left(2\frac{mv}{c} m d \sin(\hat{\theta}) + 2\frac{\hat{v}}{\lambda c} \frac{m d}{r} \sin(\hat{\theta})\right)} \quad (4.36)$$

$$\mathbf{A}_{comp} = \begin{bmatrix} \alpha_{comp,0}[0] \alpha_{comp,0}[1] \cdots \alpha_{comp,0}(L-1) \\ \vdots \\ \alpha_{comp,M-1}[0] \alpha_{comp,M-1}[1] \cdots \alpha_{comp,M-1}(L-1) \end{bmatrix} \quad (4.37)$$

$$\mathbf{X}_{comp} = (\mathbf{A} \odot \mathbf{A}_{comp}) \mathbf{S} + \mathbf{W} \quad (4.38)$$

This way, we first approximate r and θ by finding the maxima in the two dimensional power spectrum $|P(\theta, r)|$ and then approximate v in a full CPI, then use those values to compensate for the next CPI. The resulting improvements in the DoA approximation can be seen in figure 4.5.

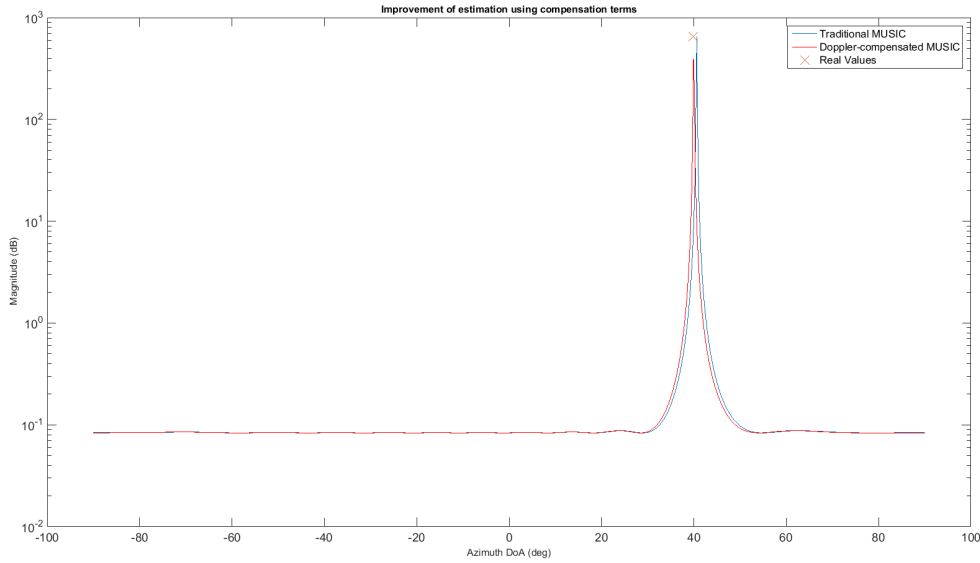


Figure 4.5: Improvement of accuracy of estimation of azimuth DoA, after using suboptimal estimates of first sweep

However, since the compensation terms depend on the range and azimuth of each target, and the incident waveforms contains combinations of all targets, this method can only work when a single target is present.

4.3.2. TIME DEPENDENT STEERING VECTORS

To overcome the problem with the previously defined method and have improved performance in multi-target scenarios, we can introduce few modifications to the steering vectors employed in modelling the array

response of existing joint delay-angle estimation algorithms.

As explained in chapter 4.2, by nature of LFMCW waveforms, we have a direct relation between instantaneous frequency of the reflected signals and time. We use the steering vectors defined in 4.31 in the joint range-azimuth estimation problem.

Similar to equation 4.6, we sort the data matrix in a single column vector. The separation of signal and noise subspaces are done as usual. Then we modify the steering vectors as follows:

$$\alpha_m[n] = e^{j2\pi\left[2\frac{m}{c}md\sin(\theta)\frac{r}{f_s} + \frac{md}{\lambda}\sin(\theta)\right]} \quad (4.39)$$

$$\alpha = [\alpha_1[0], \alpha_1[1], \dots, \alpha_1[L-1], \alpha_2[0] \dots, \alpha_M[L-1]]^T \quad (4.40)$$

$$\mathbf{b} = \mathbf{1}_M^T e^{j2\pi\left(2\frac{m}{c}r\frac{r}{f_s} + \frac{2r}{\lambda c}\right)} \quad (4.41)$$

$$\mathbf{a} = \alpha \odot \mathbf{b} \quad (4.42)$$

$$\mathbf{P}(\theta, r) = \frac{1}{\mathbf{a}^H \mathbf{U}_N \mathbf{U}_N^H \mathbf{a}} \quad (4.43)$$

To see the effects of this new algorithm, we take a look at the comparison of the single frequency and time dependent steering vectors in the case of the joint estimation problem in the figures given below.

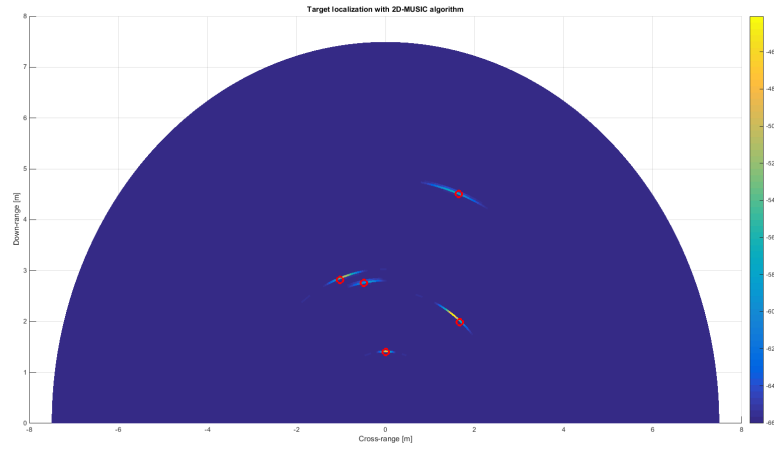


Figure 4.6: Localization of 5 randomly placed targets using 2D-MUSIC approach

The second figure, used as a baseline, contains the 2D spectrum estimation obtained by application of the algorithm presented in [21] to our simulator.

We can see that this method allows for estimation of parameters where multiple targets in different range and angle bins are present. Furthermore, the increased accuracy and resolution can be observed from both the azimuth and joint estimation plots. Further comparisons based on different radar parameters can be seen in chapter 6.

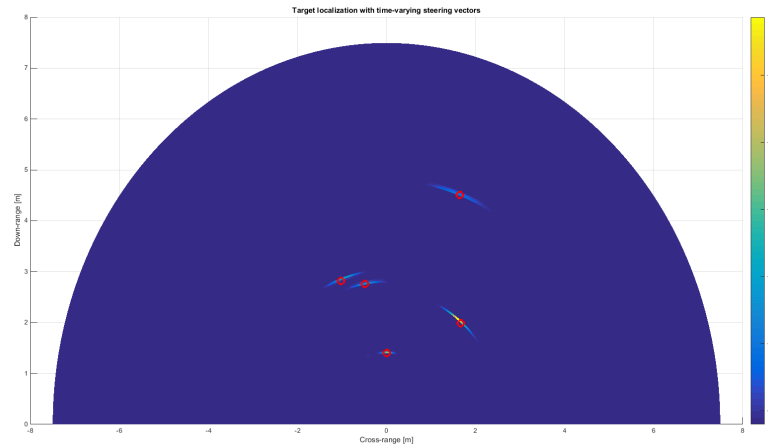


Figure 4.7: Localization of 5 randomly placed targets using proposed method

4.4. CONCLUSIONS

Upon investigation of the effects of wideband signals on parameter estimation, we provide a new signal model that is based on LFM CW radars and propose two solutions to the problem based on this model; one of them computationally less complex but cannot be implemented in a scene with multiple reflectors, and the other more complex but is applicable in all scenarios. The advantages are shown by means of comparisons to state of the art techniques; detailed performance evaluation is done in chapter 6.

5

MOVING TARGET LOCALIZATION AND JOINT RANGE-AZIMUTH-VELOCITY ESTIMATION

In this chapter, we first expand the joint estimation problem proposed in chapter 4 to a three dimensional one; estimation of angles and frequencies on the data cube shown in section 2.1. Then, we modify the data model proposed in 4.2 to take into account the movement of the targets and the effect of this on the performance of 2D and 3D estimation problem. Finally, we propose a novel way of velocity estimation taking into account the effects of near field on array processing methods.

The addition of an extra dimension in the signal model of the estimation problem is basically an extension of the two dimensional problem (range-azimuth estimation) which results only in an increase of computational complexity [16]. As additions to the existing azimuth-delay-Doppler estimation algorithms, we propose an extended version of the forward-backward spatial smoothing algorithm used in the two dimensional problem, as well as an extended look into the novel signal model of time-dependent steering vectors, this time including the effects of movement of targets and change of the Doppler shifts per array element.

5.1. RANGE-AZIMUTH-DOPPLER PROCESSING

In order to have joint estimation of the range, azimuth DoA and velocity parameters of the scatterers, we need to extend the model proposed in 4.1 to accommodate for multiple sweeps and combine it with the range-Doppler processing method described in 2.1. First, we take a look at the structure of the signal stored in the data cube

$$\mathbf{X}_{h,m,n} = \sum_{k=1}^K \gamma_k e^{j2\pi \frac{2\mu}{c} r_k \frac{n}{f_s}} e^{j \frac{2\pi}{\lambda_c} m d \sin \theta_k} e^{j2\pi \frac{2v_k}{\lambda_c} h T_s} + w_{h,m,n} \quad (5.1)$$

This simplified model takes into account only the complex exponentials containing the parameters of interest as phase information embedded on each of the dimensions of the so called radar data cube. We reshape this data cube into a vector, in a similar manner as shown in 4.6. This vector is given as

$$\mathbf{x} = [\mathbf{X}(1 \cdots H, 1, 1) \mathbf{X}(1 \cdots H, 2, 1) \cdots \mathbf{X}(1 \cdots H, L, 1) \mathbf{X}(1 \cdots H, 1, 2) \cdots \mathbf{X}(1 \cdots H, L, M)]^T \quad (5.2)$$

Forward-backward spatial smoothing can be applied in this situation for better performance under correlated signals, as well as a side benefit of reduced computational complexity. This is done as follows

$$\mathbf{C} = \begin{bmatrix} \mathbf{X}(1, 1, 1) & \cdots & \mathbf{X}(1, m_1, 1) \\ & \vdots & \\ \mathbf{X}(1, 1, m_2) & \cdots & \mathbf{X}(1, m_1, m_2) \\ \mathbf{X}(2, 1, 1) & \cdots & \mathbf{X}(2, m_1, 1) \\ & \vdots & \\ \mathbf{X}(H, 1, m_2) & \cdots & \mathbf{X}(H, m_1, m_2) \\ \mathbf{X}(1, 1, 2) & \cdots & \mathbf{X}(1, m_1, 2) \\ & \vdots & \\ \mathbf{X}(1, 1, m_2 + 1) & \cdots & \mathbf{X}(1, m_1, m_2 + 1) \\ & \vdots & \\ \mathbf{X}(H, 1, L) & \cdots & \mathbf{X}(H, M, L) \end{bmatrix} \quad (5.3)$$

$$\mathbf{R}_x = \frac{1}{p_1 p_2} (\mathbf{C}\mathbf{C}^H + \mathbf{J}\mathbf{C}\bar{\mathbf{C}}^H\mathbf{J}) \quad (5.4)$$

Autocorrelation matrix of this stacked vector shows similar structure to that of the spatio-temporal autocorrelation matrix, described in detail in chapter 4.1.

After applying SVD or EVD on this matrix, we determine the vectors spanning the noise subspace and then construct the three dimensional spectral estimate by taking the inverse of the distance of each scanning steering vector to that of the noise subspace. The scanning steering vectors are constructed as follows

$$\alpha = \exp\left(j\pi \left[\frac{2\mu}{c} m d \sin \theta t + \frac{2}{\lambda} m d \sin \theta \right]\right) \quad (5.5)$$

$$\mathbf{s} = \exp\left(j2\pi \left[2 \frac{\mu}{c} r t + 2 \frac{v}{\lambda_c} t - \frac{r}{\lambda_c} \right]\right) \mathbf{1}_L \quad (5.6)$$

$$\mathbf{d} = \exp\left(j2\pi 2 \frac{v}{\lambda_c} h T_s\right) \quad (5.7)$$

$$\mathbf{a}(v, r, \theta) = \mathbf{d} \otimes \text{vec}(\alpha \circ \mathbf{s}) \quad (5.8)$$

Using MUSIC, we can obtain a three dimensional image as follows

$$\mathbf{P}(v, r, \theta) = \frac{1}{\mathbf{a}^H \mathbf{W} \mathbf{W}^H \mathbf{a}} \quad (5.9)$$

Where \mathbf{W} contains the vectors spanning the noise subspace obtained by EVD or SVD on the autocorrelation matrix. Since it is not possible to show this resulting 3D image, we show the range-azimuth and range-Doppler parts separately (although obtained jointly) in the figures below

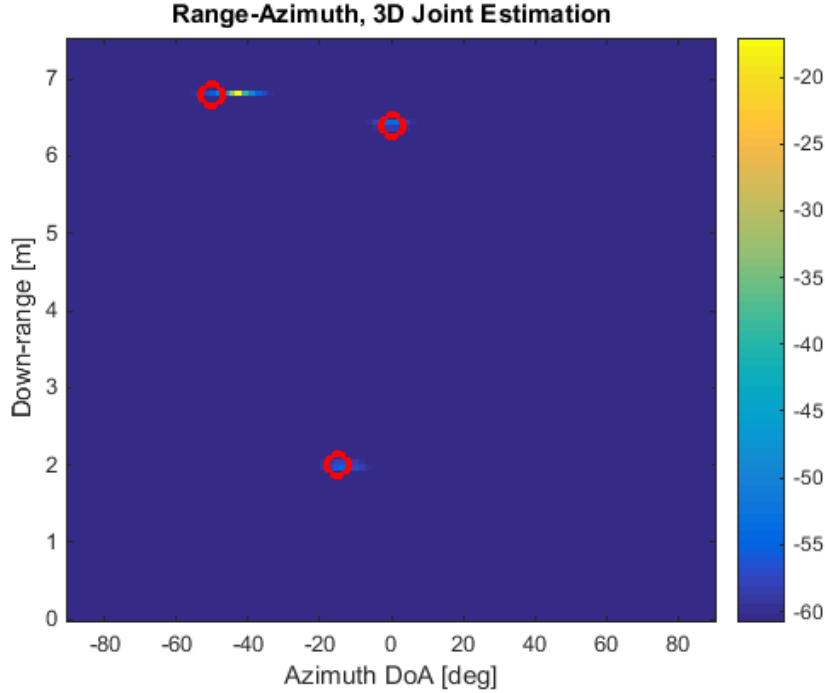


Figure 5.1: Range-Azimuth spectrum, summation of all chirps

5.2. DOPPLER SHIFT ON ARRAY ELEMENTS

When multiple moving scatterers are present, their velocity vectors and consequently, the radial velocities change for each of the elements in the array. The scatterers in this scenario are not considered to be in the far-field region, thus we don't assume plane waves and parallel line of sights for elements in the virtual array. The scenario is explained in the following figure.

We can observe this difference of observed velocity between consecutive elements of the array in the figure below

Considering this topology, and taking into account the derivation done in equation 4.32 we determine the array response as follows

$$x_1(t) = \exp \left[j2\pi \left(\frac{2r_1}{\lambda_c} + \frac{2\mu}{c} r_1 t + \frac{2v}{\lambda_c} \cos\theta_1 t \right) \right] \quad (5.10)$$

The $m - th$ element in the virtual element, after downconversion and de-ramping operations, receives the following signal

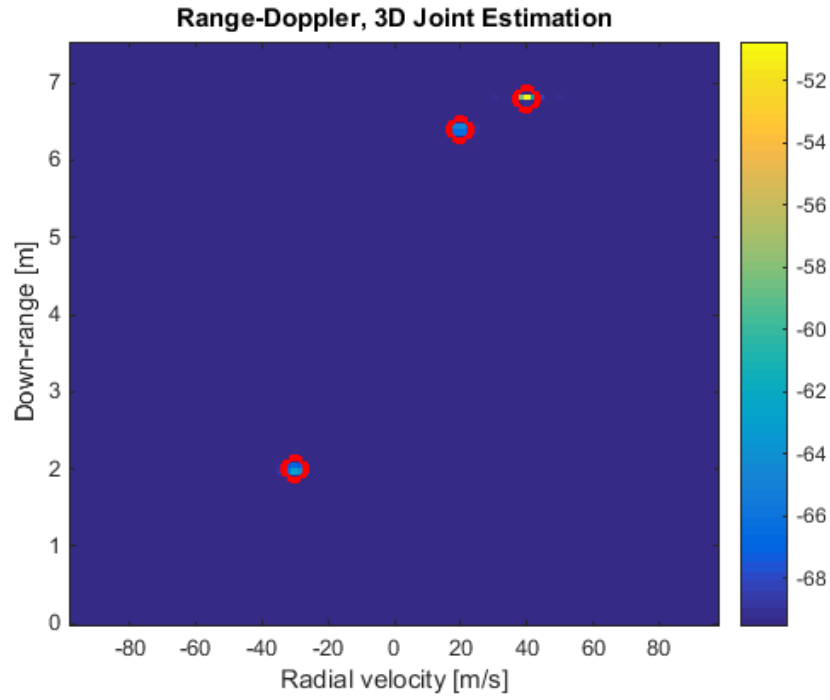


Figure 5.2: Range-Doppler plot, summation of all receiver elements

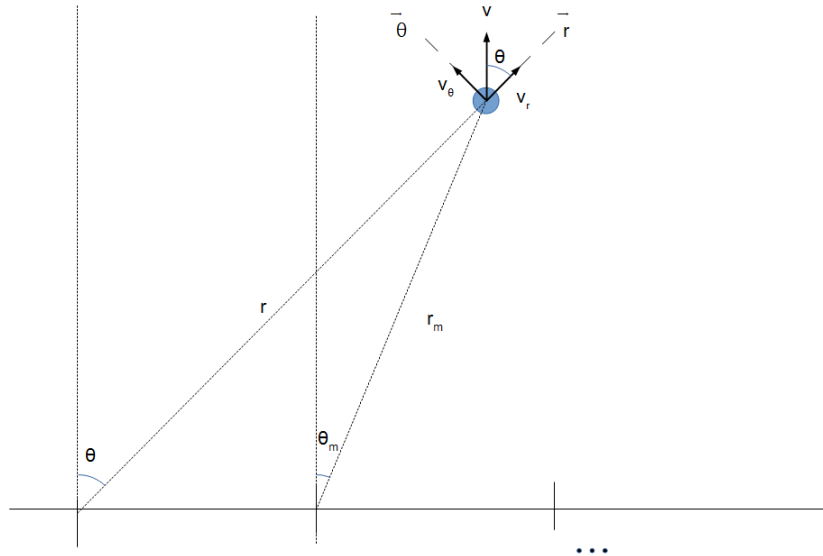


Figure 5.3: The difference of observed velocity vectors and range

$$x_m(t) = \exp \left[j2\pi \left(\frac{2r_m}{\lambda_c} + \frac{2\mu}{c} r_m t + \frac{2v}{\lambda_c} \cos\theta_m t \right) \right] \quad (5.11)$$

We know that we are working with a uniform linear array, with element spacing of d , so we need to find a relation between the time difference of arrival of wavefronts of the impinging signal to the first and m -th element of the array, that is expressed in difference of instantaneous phase and is linear with respect to m . To

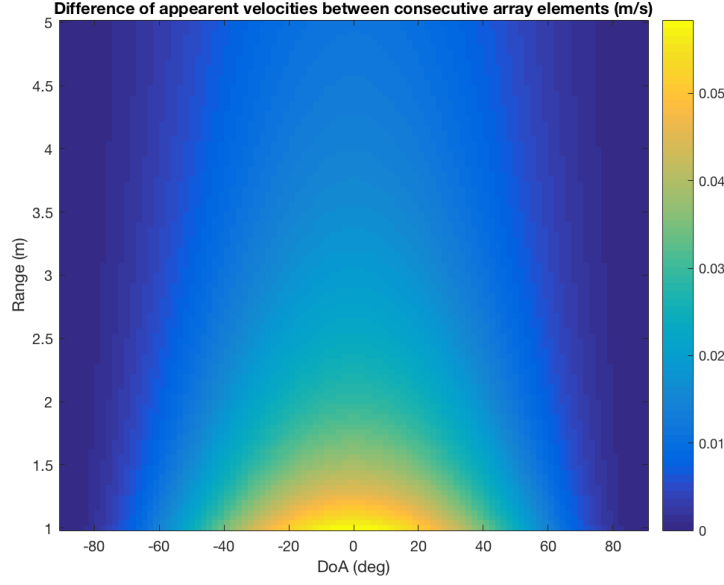


Figure 5.4: Difference of apparent velocities between consecutive array elements

do that, we simply observe

$$\alpha_m(t) = \frac{s_m(t)}{s_1(t)} = \frac{e^{j\pi\left[\left(2\frac{v}{c}r_m + 2\frac{v}{\lambda}\cos\theta_m\right)t + \frac{2r_m}{\lambda}\right]}}{e^{j\pi\left[\left(2\frac{v}{c}r_1 + 2\frac{v}{\lambda}\cos\theta_1\right)t + \frac{2r_1}{\lambda}\right]}} \quad (5.12)$$

$$= e^{j2\pi\left[\left(\frac{v}{c}(r_m - r_1) + \frac{v}{\lambda}(\cos\theta_m - \cos\theta_1)\right)t + \frac{r_m - r_1}{\lambda}\right]} \quad (5.13)$$

For simplicity, we substitute r as r_1 and θ as θ_1 . We need to be able to define $\alpha(t)$ using only θ , r , v ; terms we want to estimate and m . To that end, we observe first

$$\cos\theta_m - \cos\theta = \frac{r\cos\theta}{r_m} - \cos\theta = \frac{r\cos\theta}{\sqrt{r^2\cos^2\theta + (r\sin\theta + md)^2}} - \cos\theta \quad (5.14)$$

$$= \frac{\cos\theta}{\sqrt{1 + \frac{2md}{r}\sin\theta + \frac{m^2d^2}{r^2}\sin^2\theta}} - \cos\theta \approx \cos\theta\left(1 + \frac{2md}{r}\sin\theta\right)^{-\frac{1}{2}} - \cos\theta \quad (5.15)$$

We try to linearise this expression using Taylor series expansion of $(1+x)^n$ as follows

$$(1+x)^n = \sum_{k=0}^{\infty} (x)^k \binom{n}{k} \quad \text{for } |x| < 1 \quad (5.16)$$

Expanding the reciprocal square-root term as in Taylor series and ignoring the higher order terms, we reduce this to

$$\cos\theta_m - \cos\theta \approx -\frac{md}{r}\sin\theta \quad (5.17)$$

So what we end up is

$$\alpha_m(t) = \frac{s_m(t)}{s_1(t)} = \exp\left(j\pi\left[\frac{2v}{\lambda}\frac{md}{r}\sin\theta t + \frac{2\mu}{c}md\sin\theta t + \frac{2}{\lambda}md\sin\theta\right]\right) \quad (5.18)$$

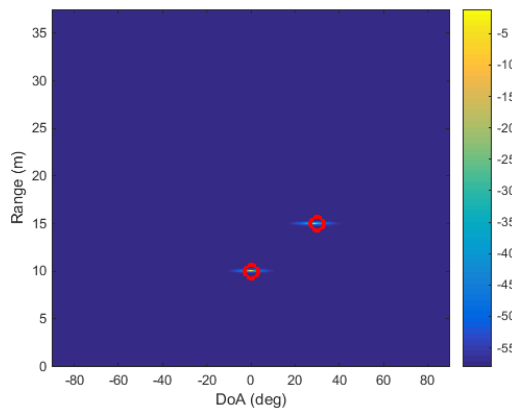
This new steering vector can be used in the both range-azimuth and range-azimuth-Doppler estimation problems defined prior.

5.3. SINGLE SWEEP VELOCITY ESTIMATION

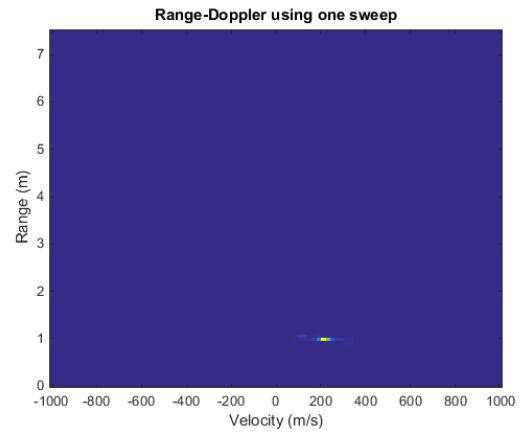
Similarly, rearranging the individual dimensions in the data cube as was done for the data matrix vectorization, and using the new signal model and steering vectors defined in equations 4.32 and 5.18, we can extend this estimation problem into 3D and find out about the velocities of the multiple moving targets.

An interesting observation from the previous chapters is that we see the emergence of the Doppler term in the array response and the steering vectors, in equation 4.32. This theoretically allows us to estimate the velocity of multiple targets in a single sweep.

By setting the steering vectors in accordance with 5.18, we can estimate range, azimuth and Doppler frequency parameters of multiple targets coherently. Using a modified MUSIC algorithm, we can obtain superresolution in all three dimensions as long as we use enough steering vectors for scanning. Since we can determine the number of steering vectors we use, the resolution of this algorithm is not limited by physical factors such as bandwidth or sweep time but by the fact that we need to differentiate between signal and noise eigenvectors for the algorithm to run, which is a detection problem that depends on the SNR.



(a) Range-Azimuth estimation using 500 steering vectors for both dimensions



(b) Range-Doppler processing using only one sweep

5.4. CONCLUSIONS

In this chapter, we present the azimuth-delay-Doppler problem as a three dimensional joint spectral estimation problem. Using a modified version of the Forward-backward spatial smoothing algorithm, we reduce the computational complexity and solve the problem using traditional MUSIC algorithm based on the single fre-

quency steering vectors which does not take into account the intra-pulse Doppler shifts and their difference with respect to different elements on the array. We then propose a new signal model, similarly formulated as in previous chapter, to take into account these effects. As a side note, we observe that using the new signal model, theoretically, it is possible to estimate Doppler shifts using only a single sweep, which reduces the dimensionality of the problem significantly. However, as stated, due to the restrictions on the element spacings and the nature of the operating frequencies, the phase shifts that are meant to be observed are small in magnitude: less than the available resolution using MUSIC algorithm for reasonable velocities. We only managed to distinguish Doppler velocities using speeds much higher than what is observed in automotive radar settings.

6

PERFORMANCE EVALUATION

In this chapter, we focus on the comparison of performance with respect to accuracy and resolution of the algorithms introduced in the previous chapters. It is shown in previous chapters that we have indeed achieved resolutions in three domains that are finer than what is available using simple FFT based methods, so we compare the performance with respect to the state of the art joint range-azimuth estimation methods.

All comparisons to the so called 2D MUSIC algorithm are done by implementing the algorithm given in [21] in our simulator and running multiple times with randomized parameters.

6.1. EFFECT OF SNR ON ESTIMATION ACCURACY

Both the widely used signal models and the newly defined ones in this thesis, in chapters 4 and 5, a noise model of AWGN is assumed, for simplicity of derivations. Even though in our simulator, we define multiple sources of noise (phase noise, thermal noise etc.) and consider the effects of clutter, in order to be more accurate, since it is not feasible to reduce the effects of all of them in a single parameter to be compared, for these set of comparisons, we revert back to the simpler signal models. We run multiple simulations for each SNR value, ranging from -20 dB to 0 dB with steps of 5 dB, with randomly placed targets and take the mean square error of both range and azimuth estimations; both using the newly developed algorithm explained in 5.3 (although omitting the velocity estimation part, as our comparison model does not include estimation of velocities) and the joint 2D estimation algorithm given in [21]. MATLAB quick 1-D linear interpolation algorithm was used to interpolate the RMSE values in the intermediate SNR figures.

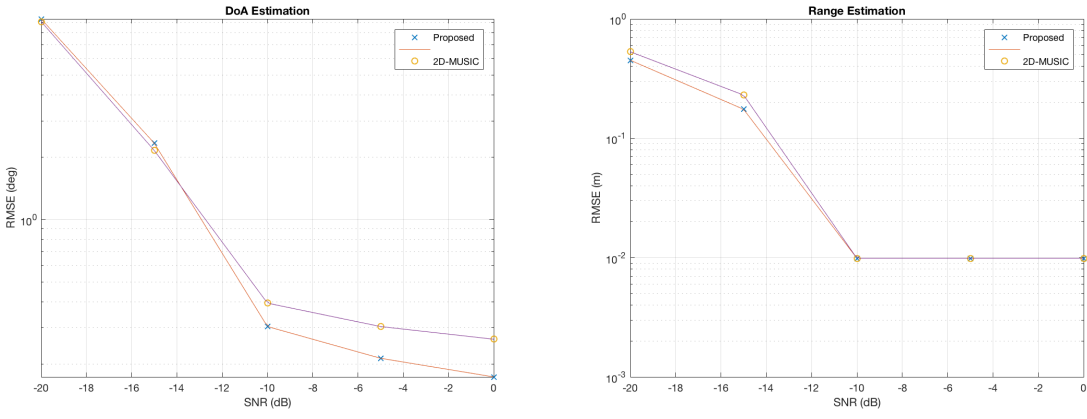
As for a theoretical limit, we take a look at the Cramér-Rao lower bound (CRLB) of the MUSIC algorithm

for estimation of azimuth DoA parameters, formulated in [23]. For sufficiently large number of samples for the estimate covariance matrix and for sufficiently large number of antenna elements, the CRLB is given as

$$\frac{6}{m^3 N} \frac{1}{SNR} \quad (6.1)$$

Where m is the number of elements in the (virtual) array (in our case, we need to consider the effective array length after the FB-SS algorithm), N is the number of time samples per sweep and SNR is the signal-to-noise ratio, in linear scale. However, this only gives us the bound for the parameter $2\pi \frac{\lambda_c}{d} \sin(\theta)$, as such, an arcsin operation needs to be performed on this figure, as shown in [22].

We chose MUSIC as our estimation method because of its known sub-par performance on lower SNR values, in order to see what sort of advantages our model has in such cases.



(a) DoA Estimation Error

(b) Range Estimation Error

Figure 6.1: Effect of SNR on parameter estimation

We can observe that at low SNR values, the performance of both algorithms is poor and there is not much difference in performance; that is due to the limitations of MUSIC based spectrum estimation methods. Furthermore, we see an almost negligible improvement over errors in range estimation, however, the performance increase in DoA estimation is quite significant. The reason of this negligible gain in range domain is that our new signal model changes the 2D and 3D steering vector based on the array response, thus, very little change occurs in the range domain.

For the parameters used in these set of experiments, we obtain a CRLB of 0.1368 degrees in azimuth DoA estimation at 0 dB SNR, the RMSE of azimuth DoA estimation of the newly proposed algorithm is 0.1735 at 0 dB SNR and the RMSE of the joint 2D MUSIC based estimator is 0.2639 at 0 dB SNR.

6.2. EFFECT OF SWEEP BANDWIDTH ON ESTIMATION ACCURACY

Another important parameter for an automotive radar system is the sweep bandwidth. As we have discussed in chapter 4, for transmit waveforms containing multiple (infinite) frequency components, the performance of beamforming techniques drop significantly compared to single frequency sources. We expect to see a

trend of negligible improvements in low fractional bandwidth cases but significant improvement as fractional bandwidth increases.

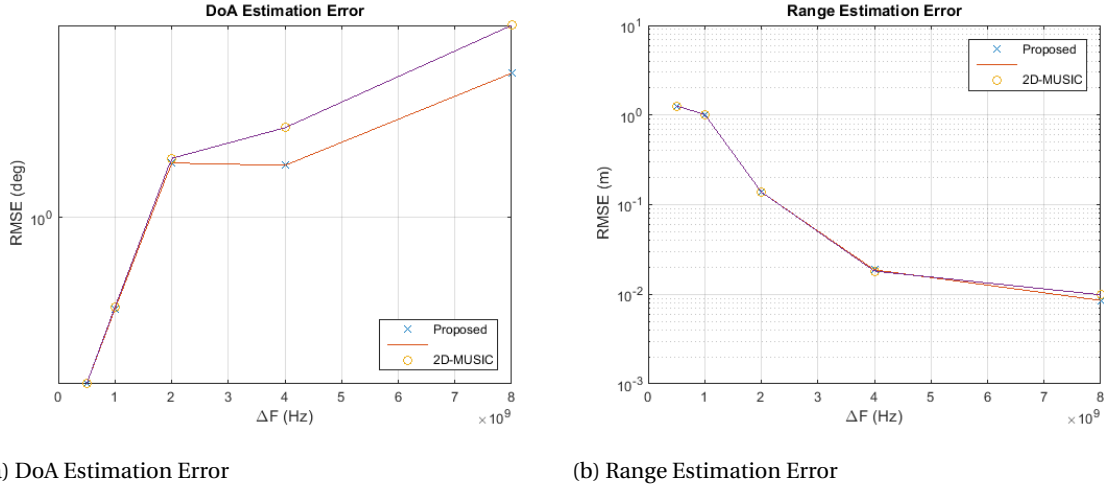


Figure 6.2: Effect of sweep bandwidth on parameter estimation

Here we see that as the sweep bandwidth of the transmit signal increases, the difference in RMSE also increases. This is due to the fact that as fractional bandwidth increases, the validity of the narrow band assumption decreases.

6.3. EFFECT OF POSITION OF SCATTERERS ON ESTIMATION ACCURACY

The new signal model has dependence of range as well as velocity in the derivation of the array response. Theoretically, we expect to see more erroneous estimations using the single frequency and velocity independent steering vectors in closer ranges, due to the fact that difference of observed Doppler frequencies per element increases as the scatterer is nearer to the array. However, since the frequency terms containing range dependence have less magnitude than the terms containing the change of wavelength during the sweep (a difference of usually two orders of magnitude), the difference might not be observable or simply lost within noise floor.

Here, we run multiple simulations under two conditions, first we place many random targets in the scene and just sort the azimuth estimation errors according to their ranges and for the second case, we fix the range of the targets and do multiple runs of the simulation and compare the range estimation errors. In both cases, all other parameters such as SNR, sweep bandwidth, target velocities etc. are kept constant.

Considering the data from these trials, we observe what was hypothesised; minor improvements in cases when target is close by and the absolute value of the azimuth angle is smaller.

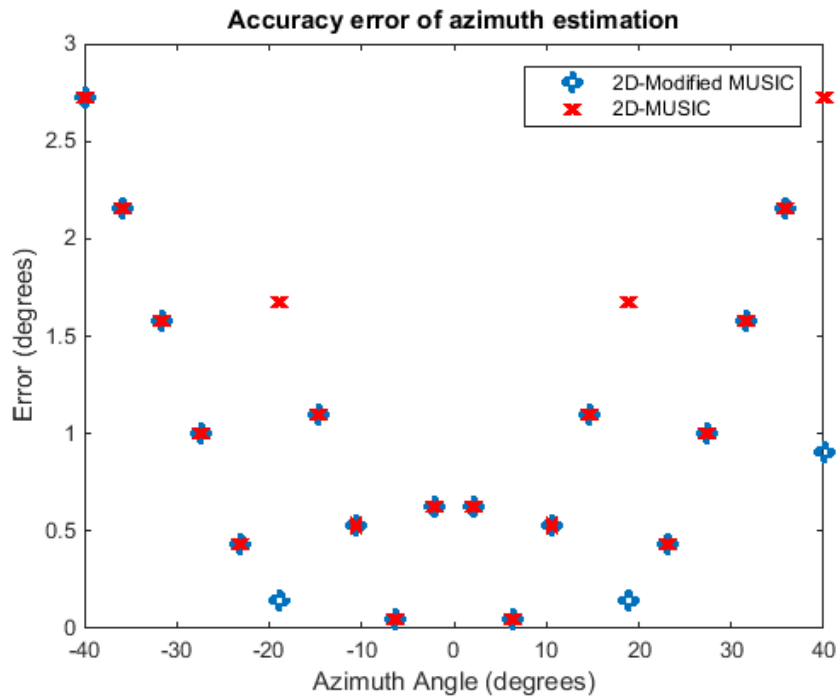


Figure 6.3: Scatterplot of DoA estimation errors, random ranges

6.4. APPLICATION ON EXPERIMENTAL DATA

Finally, in order to test the validity of our models, we use real life data, taken from the NXP Dolphin automotive radar. The operating parameters of this radar is given in the table below.

Parameter	Value	Unit
Chirp Bandwidth	250	MHz
Chirp Time	23.8	μs
Sample Frequency	40	MHz
Number of Chirps	64	[]
Carrier Frequency	78.57	GHz

Table 6.1: NXP Radar Parameters

The radar in question has 3 transmitter and 4 receiver elements, using time domain multiplexing for achieving orthogonality of transmit signals. There is a stationary target approximately 20m away and a moving target approximately 60m away, during the observation period.

Due to a limitation in hardware, it was not possible to obtain phase information of array elements; the output data was only in single channel (in-phase) mode. Therefore azimuth estimation was not possible, however, range-Doppler estimation using the methods defined in chapter 5 (not single sweep but 3D joint estimation method) was possible. Figures below give the processing of the same data, first with the 2D FFT based method that was previously used and secondly the method defined in 5.1; however ignoring the az-

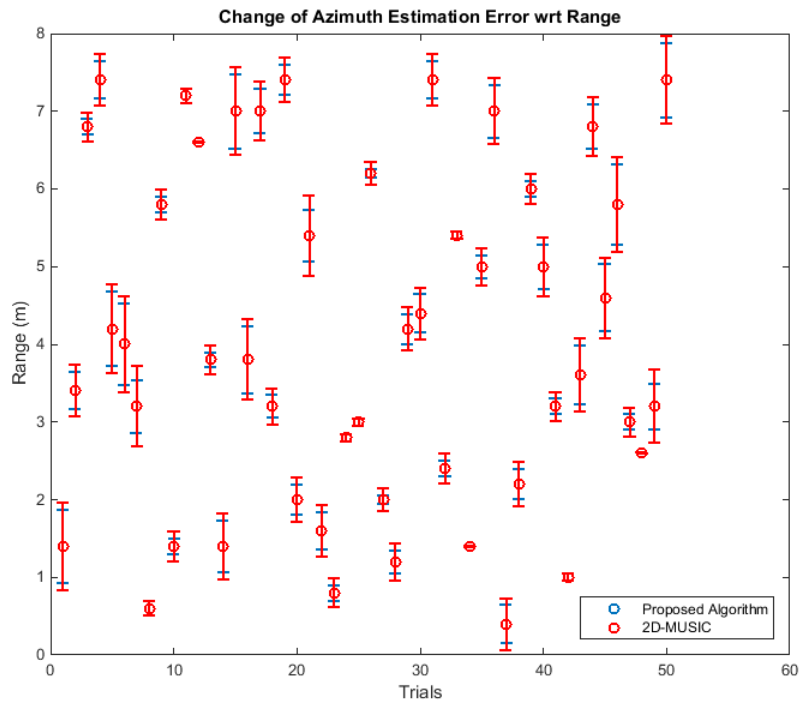


Figure 6.4: Change of azimuth error with respect to range of scatterer over multiple random experiments

imuth estimation parts by just using a single transmit-receive pair, due to the hardware limitations.

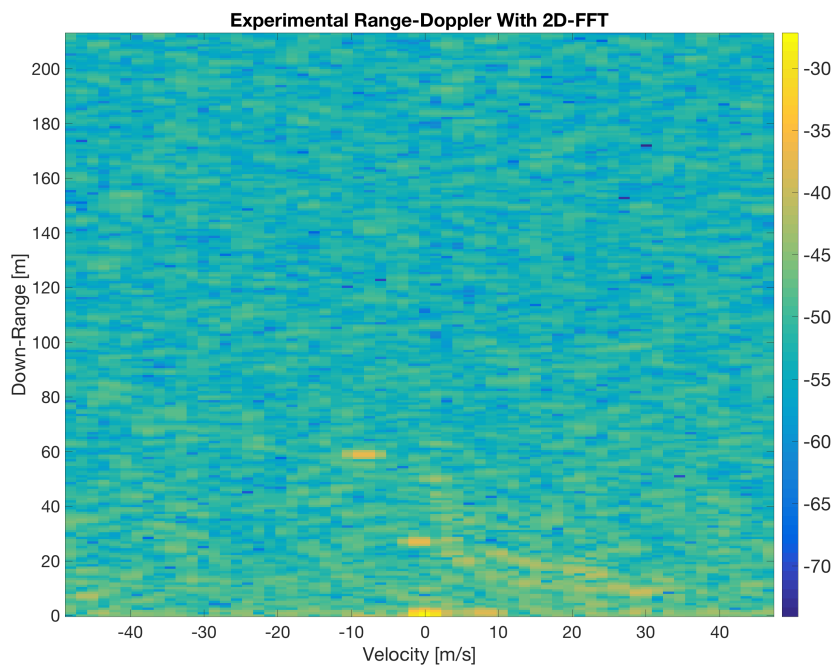


Figure 6.5: Range-Doppler processing, 2D FFT

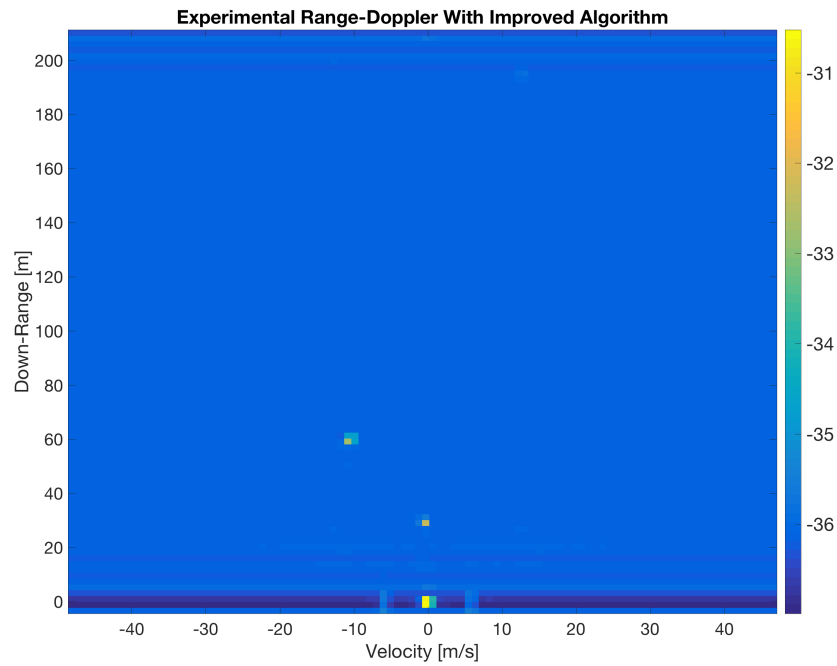


Figure 6.6: Range-Doppler processing, MUSIC

6.5. CONCLUSIONS

As a result of multiple experimental runs of our radar simulator under varying conditions, we observe that the MUSIC based joint estimation method offers better accuracy when used with the novel signal model and steering vectors defined in previous chapter. We see an improvement of 0.1 degrees of RMSE of the azimuth DoA estimation at 0 dB SNR. Furthermore, we see a more drastic effect of the sweep bandwidth on the RMSE of DoA estimation; with 1 GHz sweep bandwidth (maximum allocated for the 77 GHz band by ETSI), the discrepancy is only 0.048 degrees, whereas with 4 GHz sweep bandwidth (maximum allocated for the 79 GHz band by ETSI), we see an improvement of 0.407 degrees and for 8 GHz sweep bandwidth, we see an improvement of 0.995 degrees RMSE.

7

CONCLUSIONS

The goal of this project was twofold, first investigate super-resolution algorithms for joint range-azimuth-velocity estimation in FMCW automotive radar applications where multiple targets of interest exist. Secondly, we were to investigate the effects of wideband signals and movement of targets on the performances of such super-resolution algorithms.

In order to achieve this, an accurate and detailed simulator was to be implemented. At first, a third party radar signal processing simulator was intended to be used. For this purpose, a C++ based simulator called FERS (Flexible Extensible Radar Simulator) was investigated. However, due to the fact that MIMO processing methods were not fully realized and the simulator focused more on pulsed radars, and had many errors using continuous waveforms, this was discarded.

The new simulator was done purely on MATLAB. It involves full baseband signal processing, accurate noise and clutter modelling, accurate MIMO processing and hardware component models. However, since it was computationally complex to run this model every time, we first compared the validity of more simplistic signal models with the simulator, and did the derivations of new models on said models. However, all processing results are done on the data that is taken from this simulator, including the experiments in chapter 6.

Then we investigate the effects of wideband LFM CW signals on joint range-azimuth estimation methods, and come up with a new signal model that is based on such transmit waveforms. We show the problems arising due to using a model designed for single frequency waveforms while using FMCW waveforms. We derive two ways of overcoming the problems, however since one of them requires a single target to be present, we focus more on the solution of time-dependent steering vectors. We implement this new signal model on existing super-resolution algorithms and show the improved performance.

Finally, we investigate both the three dimensional joint estimation problem and the effects of existence of multiple moving targets on both the range-azimuth and range-azimuth-velocity estimation problems. We derive a more detailed signal model that takes into account the effect of (radial) movement of the targets in array processing methods. Furthermore, we develop a novel algorithm for joint estimation of range, azimuth and velocity parameters and achieve super-resolution in all three domains. Finally, due to the occurrence of velocity terms in the array response, we propose a novel way of range azimuth and velocity estimation using only a single LFM CW chirp.

After the development of these methods, we show the performance improvements by comparing the estimation errors of parameters using state-of-the-art super-resolution methods, both with the old signal model and the newly developed one. We observe improvements in both range and azimuth estimation in high SNR and high chirp bandwidth scenarios; more than 2 degrees RMSE in azimuth and 50cm in range.

Finally, we show the validity of our joint estimation algorithm on real-life data taken from NXP automotive radar. Due to the limitations of the hardware, we are unable to obtain range estimation but we show that the range doppler processing works and has improved resolution.

7.1. FUTURE WORKS

There are multiple ways to extend this work, based on the newly developed signal model and the processing algorithms. Due to time limitations, estimation of velocity in two directions was not done, we only consider the targets that are moving in a perpendicular direction from the array (parallel to the array normal) and we only estimate the radial velocity vectors. Using different array topologies or multistatic radar configurations, it is theoretically possible to estimate velocity vectors in range and cross-range directions.

Furthermore, a more detailed model can be devised to accommodate the targets that are moving in any direction in the x-y plane.

More sparse arrays theoretically can yield better performance in single chirp estimation methods. Moreover, due to the fact that we take into account the changes of observed Doppler frequency over the array, theoretically, the degradation of performance due to ignoring the movement of the targets increases as the aperture size as well as the array spacings increases.

Finally, an investigation into different waveforms (up and down FMCW chirps, stepped frequency CW radars etc.) can be done in order to create better signal models suited for such waveforms; since in our derivations, we strictly consider the LFM CW transmit waveform and base our model on this fact.

BIBLIOGRAPHY

- [1] W. L. Melvin and J. A. Scheer, *Principles of Modern Radar: Advanced Techniques* (SciTech Publishing, 2012).
- [2] M. A. Richards, J. A. Scheer, and W. A. Holm, *Principles of Modern Radar: Basic Principles* (SciTech Publishing, 2010).
- [3] V. Winkler, *Range doppler detection for automotive fmcw radars*, in *2007 European Radar Conference* (2007) pp. 166–169.
- [4] W. Roberts, P. Stoica, J. Li, T. Yardibi, and F. A. Sadjadi, *Iterative adaptive approaches to mimo radar imaging*, *IEEE Journal of Selected Topics in Signal Processing* **4**, 5 (2010).
- [5] L. Tzafri and A. J. Weiss, *High-resolution direct position determination using mvdr*, *IEEE Transactions on Wireless Communications* **15**, 6449 (2016).
- [6] Y. S. Yoon, M. G. Amin, and F. Ahmad, *Mvdr beamforming for through-the-wall radar imaging*, *IEEE Transactions on Aerospace and Electronic Systems* **47**, 347 (2011).
- [7] P. Stoica, H. Li, and J. Li, *A new derivation of the apes filter*, *IEEE Signal Processing Letters* **6**, 205 (1999).
- [8] J. Li and P. Stoica, *Mimo radar diversity means superiority*, in *MIMO Radar Signal Processing* (Wiley-IEEE Press, 2009) pp. 1–64.
- [9] A. Jakobsson and P. Stoica, *Combining capon and apes for estimation of spectral lines*, *Circuits, Systems and Signal Processing* **19**, 159 (2000).
- [10] W. Xia and Z. He, *Multiple-target localization and estimation of mimo radars using capon and apes techniques*, in *2008 IEEE Radar Conference* (2008) pp. 1–6.
- [11] R. Schmidt, *Multiple emitter location and signal parameter estimation*, *IEEE Transactions on Antennas and Propagation* **34**, 276 (1986).
- [12] F. Belfiori, W. van Rossum, and P. Hoogeboom, *Coherent mimo array design with periodical physical element structures*, *IEEE Antennas and Wireless Propagation Letters* **10**, 1341 (2011).
- [13] G. O. Manokhin, Z. T. Erdyneev, A. A. Geltser, and E. A. Monastyrrev, *Music-based algorithm for range-azimuth fmcw radar data processing without estimating number of targets*, in *Microwave Symposium (MMS), 2015 IEEE 15th Mediterranean* (2015) pp. 1–4.

- [14] R. Roy, A. Paulraj, and T. Kailath, *Estimation of signal parameters via rotational invariance techniques - esprit*, in *Military Communications Conference - Communications-Computers: Teamed for the 90's, 1986. MILCOM 1986. IEEE*, Vol. 3 (1986) pp. 41.6.1–41.6.5.
- [15] M. D. Zoltowski and K. T. Wong, *Esprit-based 2-d direction finding with a sparse uniform array of electromagnetic vector sensors*, *IEEE Transactions on Signal Processing* **48**, 2195 (2000).
- [16] T. Strohmer and B. Friedlander, *Analysis of sparse {MIMO} radar*, *Applied and Computational Harmonic Analysis* **37**, 361 (2014).
- [17] D. B. Leeson, *A simple model of feedback oscillator noise spectrum*, *Proceedings of the IEEE* **54**, 329 (1966).
- [18] G. Babur, O. A. Krasnov, A. Yarovoy, and P. Aubry, *Nearly orthogonal waveforms for mimo fmcw radar*, *IEEE Transactions on Aerospace and Electronic Systems* **49**, 1426 (2013).
- [19] G. Xu, R. H. Roy, and T. Kailath, *Detection of number of sources via exploitation of centro-symmetry property*, *IEEE Transactions on Signal Processing* **42**, 102 (1994).
- [20] T.-J. Shan, M. Wax, and T. Kailath, *On spatial smoothing for direction-of-arrival estimation of coherent signals*, *IEEE Trans. Acoust. Speech Signal Process* **33**, 806 (1985).
- [21] F. Belfiori, W. van Rossum, and P. Hoogeboom, *2d-music technique applied to a coherent fmcw mimo radar*, in *Radar Systems (Radar 2012), IET International Conference on* (2012) pp. 1–6.
- [22] D. Oh and J. H. Lee, *Low-complexity range-azimuth fmcw radar sensor using joint angle and delay estimation without svd and evd*, *IEEE Sensors Journal* **15**, 4799 (2015).
- [23] P. Stoica and A. Nehorai, *Music, maximum likelihood and cramer-rao bound: further results and comparisons*, in *International Conference on Acoustics, Speech, and Signal Processing*, (1989) pp. 2605–2608 vol.4.